



**QUEEN'S
UNIVERSITY
BELFAST**

3D-printed hydrogels based on amphiphilic chitosan derivative loaded with levofloxacin for wound healing applications

Lazaridou, M., Moroni, S., Klonos, P., Kyritsis, A., Bikiaris, D. N., & Lamprou, D. A. (2024). 3D-printed hydrogels based on amphiphilic chitosan derivative loaded with levofloxacin for wound healing applications. *International Journal of Polymeric Materials and Polymeric Biomaterials*. Advance online publication. <https://doi.org/10.1080/00914037.2024.2314610>

Published in:

International Journal of Polymeric Materials and Polymeric Biomaterials

Document Version:

Publisher's PDF, also known as Version of record

Queen's University Belfast - Research Portal:

[Link to publication record in Queen's University Belfast Research Portal](#)

Publisher rights

Copyright 2024 The Authors.

This is an open access article published under a Creative Commons Attribution-NonCommercial-NoDerivs License (<https://creativecommons.org/licenses/by-nc-nd/4.0/>), which permits distribution and reproduction for non-commercial purposes, provided the author and source are cited.

General rights

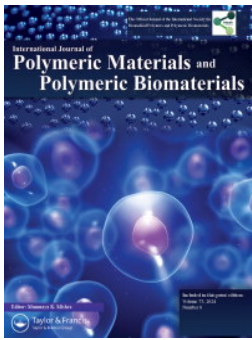
Copyright for the publications made accessible via the Queen's University Belfast Research Portal is retained by the author(s) and / or other copyright owners and it is a condition of accessing these publications that users recognise and abide by the legal requirements associated with these rights.

Take down policy

The Research Portal is Queen's institutional repository that provides access to Queen's research output. Every effort has been made to ensure that content in the Research Portal does not infringe any person's rights, or applicable UK laws. If you discover content in the Research Portal that you believe breaches copyright or violates any law, please contact openaccess@qub.ac.uk.

Open Access

This research has been made openly available by Queen's academics and its Open Research team. We would love to hear how access to this research benefits you. – Share your feedback with us: <http://go.qub.ac.uk/oa-feedback>



3D-printed hydrogels based on amphiphilic chitosan derivative loaded with levofloxacin for wound healing applications

Maria Lazaridou, Sofia Moroni, Panagiotis Klonos, Apostolos Kyritsis, Dimitrios N. Bikiaris & Dimitrios A. Lamprou

To cite this article: Maria Lazaridou, Sofia Moroni, Panagiotis Klonos, Apostolos Kyritsis, Dimitrios N. Bikiaris & Dimitrios A. Lamprou (13 Feb 2024): 3D-printed hydrogels based on amphiphilic chitosan derivative loaded with levofloxacin for wound healing applications, International Journal of Polymeric Materials and Polymeric Biomaterials, DOI: [10.1080/00914037.2024.2314610](https://doi.org/10.1080/00914037.2024.2314610)

To link to this article: <https://doi.org/10.1080/00914037.2024.2314610>



© 2024 The Author(s). Published with license by Taylor & Francis Group, LLC.



[View supplementary material](#)



Published online: 13 Feb 2024.



[Submit your article to this journal](#)



Article views: 839



[View related articles](#)



[View Crossmark data](#)

3D-printed hydrogels based on amphiphilic chitosan derivative loaded with levofloxacin for wound healing applications

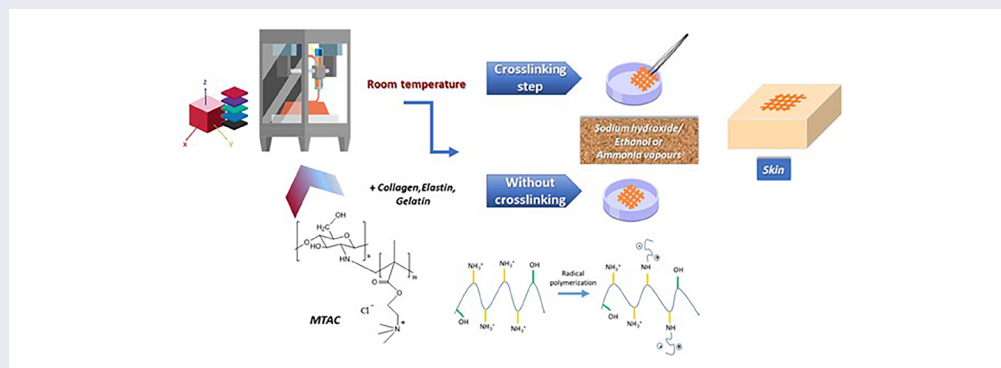
Maria Lazaridou^{a,b}, Sofia Moroni^a, Panagiotis Klonos^c, Apostolos Kyritsis^c, Dimitrios N. Bikiaris^b and Dimitrios A. Lamprou^a

^aSchool of Pharmacy, Queen's University Belfast, Belfast, United Kingdom; ^bDepartment of Chemistry, Aristotle University of Thessaloniki, Thessaloniki, Greece; ^cDepartment of Physics, National Technical University of Athens, Athens, Greece

ABSTRACT

Skin wounds not only cause physical pain to patients but also pose an economic burden to society. Consequently, effective approaches to promote skin repair remain a challenge. Specifically, chitosan-based hydrogels are ideal candidates to promote wound healing at different stages and while diminishing the factors that impede this process (such as excessive inflammatory and chronic wound infection). Furthermore, the unique biological properties of a chitosan-based hydrogel enable it to serve as both a wound dressing and a drug delivery system (DDS). In the present work, chitosan (CS) graft copolymer with [2-(methacryloyloxy)ethyl] trimethyl ammonium chloride (CS-MTAC), a cationic monomer with promising antibacterial properties, was synthesized. The successful synthesis of the copolymer was confirmed, while it was studied for its swelling ability and water absorption capacity, as well as for its biocompatibility and antibacterial properties. Expecting to improve its printability, the copolymer was blended with elastin (EL), collagen (COL), and increasing concentrations of gelatin (GEL). The hydrogel with 6% w/v CS, 4% w/w EL, 4% w/w COL and 1% w/v GEL was selected for its potential to be 3D-printed and was neutralized with ammonia vapors or ethanol/sodium hydroxide solution and loaded with levofloxacin. The feasibility of CS-MTAC/EL/COL/GEL bioink, loaded with Levo, as a suitable candidate for wound healing and drug delivery applications, has been demonstrated.

GRAPHICAL ABSTRACT



ARTICLE HISTORY

Received 4 December 2023
Accepted 1 February 2024

KEYWORDS

3D printing; cationic acrylate monomer; chitosan; collagen; elastin; gelatin; hydrogels; levofloxacin; wound healing


1. Introduction

Skin damages, like acute and chronic wounds related to chronic diseases, burns or post-surgical trauma are of high significance in clinical practice because of their tendency to be colonized by bacteria [1]. Healthy skin is essential for maintaining homeostasis, thermoregulation and the protection of the human body against infection avoiding microbial growth and the introduction of harmful microorganisms.

Since wounds are a major health concern having an impact on the lives of millions of people there is a demand for the fabrication of novel skin dressings in order to control and treat them [2]. Researchers have suggested that reducing the number of bacteria in wounds with topical administration of antibiotics can make infections easier to handle [3].

3D printing (3DP) has emerged as a promising tool in tissue engineering and drug delivery applications, due to its ability to create complex, customizable structures with

CONTACT Dimitrios N Bikiaris  dbic@chem.auth.gr  Department of Chemistry, Aristotle University of Thessaloniki, Thessaloniki, Greece
Dimitrios A Lamprou  d.lamprou@qub.ac.uk  School of Pharmacy, Queen's University Belfast, Belfast, United Kingdom

 Supplemental data for this article can be accessed online at <https://doi.org/10.1080/00914037.2024.2314610>.

© 2024 The Author(s). Published with license by Taylor & Francis Group, LLC.

This is an Open Access article distributed under the terms of the Creative Commons Attribution-NonCommercial-NoDerivatives License (<http://creativecommons.org/licenses/by-nc-nd/4.0/>), which permits non-commercial re-use, distribution, and reproduction in any medium, provided the original work is properly cited, and is not altered, transformed, or built upon in any way. The terms on which this article has been published allow the posting of the Accepted Manuscript in a repository by the author(s) or with their consent.

precise control over shape, size, and composition. In recent years, 3DP technique have been applied to several synthetic and natural polymers, including poly(vinyl alcohol) (PVA) [4], polycaprolactone (PCL) [5], poly(lactic acid) (PLA) [6], nanocellulose [7] or chitosan (CS) [8]. Among them, CS is the only cationic natural polysaccharide, derived from the exoskeletons of crustaceans such as shrimps and crabs. Its properties, such as biocompatibility, biodegradability, ability to promote cell adhesion and proliferation make it an attractive material for tissue engineering applications [9,10]. Additionally, chitosan has been shown to have antimicrobial activity, which can also help to prevent several kinds of infections [11,12].

CS possesses two functional groups, a hydroxyl and an amino group, making it possible to be derivatized with several monomers to expand its properties [13]. Cationic monomers are promising candidate for the development of antimicrobial agents [14]. The main positively charged moieties in these natural or synthetic structures are quaternary ammonium groups which react with cytoplasmic membrane (lipid or protein) causing membrane disorganization and other damages to the bacterial cell [15]. Modifying CS with cationic monomers can improve the properties of CS hydrogels for tissue engineering applications such as solubility and swelling. Additionally, CS could be used as a blend with other materials (e.g., gelatin, alginate, chondroitin sulfate, pectin) in order to increase viscosity values, an important parameter in the 3DP technique.

GEL contains specific amino acidic residues such as Arg-Gly-Asp (RGD) in its sequence [16], existing also in the proteins of extracellular matrix [17] and is involved in numerous physiological functions. For this reason, the combination of chitosan with GEL has been investigated for various biomedical applications like wound healing [18] or drug delivery [19]. Moreover, GEL is known for its ability to promote cell adhesion and growth.

EL is an extracellular protein that provides the elasticity to the tissues, such as blood vessels, ligaments, the lungs, and skin [20]. Researchers have also explored the use of EL in tissue-engineered skin [21], heart valves [22], and cartilage constructs [23]. The introduction of elastin in PCL scaffolds led to more hydrophilic materials with enhanced biocompatibility [24]. At the same time Grover et al. proved that adding both insoluble and soluble EL increased the tensile strength of a collagen porous scaffold [25] while EL-based biomaterials exhibit great potential for use as hydrogel scaffolds for the regeneration of damaged cartilage [25]. Additionally, it was confirmed that elasin induces cell migration and proliferation during wound healing. In the same direction, collagen protein was added as a biocompatible and biodegradable component of the human extracellular matrix (ECM) but also actively participate in the wound healing process [26].

Hence, the aim of the present study was the preparation of a chitosan derivative grafted with cationic monomer, MTAC, and then the development of the biocompatible inks CS-MTAC based designed for 3DP applications. In order to optimize its printability, CS-MTAC was combined with GEL, COL and EL taking advantage of their own properties that could also promote

the wound healing process. An examination of the new CS derivative and its 3DP structures was followed by drug loading of the optimized 3DP patch. Recently, CS was combined with the polymerized form of MTAC in order to prepare dressings with self-healing properties [27]. Heydarifard *et al.* studied the impact of counter ions of cationic monomers, among them MTAC, during radical polymerization with chitosan using another initiator, ceric ammonium nitrate, at different conditions (50 °C, 5h, pH = 7) for removing dyes from solutions [28]. To the best of our knowledge, the use of CS-MTAC copolymer in 3DP field, as well as the specific compositions of materials was examined for the first time.

2. Materials and methods

2.1. Materials

CS with medium molecular weight (310,000–375,000 Da) and degree of deacetylation >75% was supplied from Sigma Aldrich Co (St. Louis, MO, USA) and [2-(methacryloyloxy) ethyl] trimethylammonium chloride (MTAC) stabilized with 150–200ppm 4-methoxyphenol from Alfa Aesar. Gelatin from bovine skin (type B) was purchased from Serva, elastin and Collagen type I from bovine Achilles tendon were supplied by Sigma-Aldrich (St. Louis, MO, USA). Sodium hydroxide (NaOH) was purchased from Chem-Lab NV (Zedelgem, Belgium) Merck (KGaAn Darmstadt, Germany), Ethanol Denatured (EtOH) from Plynarenska (Bratislava), Ammonia solution (NH₃) and Levofloxacin (levo) (99.99% purity) was kindly donated by Pharmathen SA. All other reagents used were of analytical grade.

2.2. Synthesis of CS-MTAC copolymer

The CS-MTAC copolymer derivative was synthesized by free radical polymerization with similar procedure to previous reports, where chitosan was modified with [2-(methacryloyloxy)ethyl] trimethylammonium chloride (MTAC) using another radical initiator, potassium persulfate [29]. Briefly, 10 g of neat chitosan (60 mmol) was dissolved in aqueous solution of acetic acid (2% v/v) and then 2,32 ml of [2-(methacryloyloxy) ethyl] trimethylammonium chloride (12 mmol) was added to the solution, in the presence of ammonium persulfate initiator (0.3 mmol based on the monomer). The grafting reaction took place at 60 °C, over 2h, under a nitrogen atmosphere and with continuous mechanical stirring. A viscous liquid was obtained, and pH was increased to approximately 6.5 by the dropwise addition of a 1 M aqueous solution of NaOH. The resulting suspension was purified via dialysis against water (cellulose membrane with a molecular weight cutoff of 12400), in order to remove MTAC homopolymers that might have been formed and freeze-dried under reduced pressure at –60 °C. The copolymer was further purified by Soxhlet extraction with methanol. The grafting percentage, (GP), and grafting efficiency, (GE), were calculated according to Eqs. 1 and 2, respectively.

$$GP = [(M_{fin} - M_{in}) / M_{in}] \times 100 \quad (1)$$

$$GE = (W_2 - W_1) / W_3 \quad (2)$$

where, M_{in} and M_{fin} are the mass of CS before and after the grafting process whereas, W_1 , W_2 , and W_3 are the initial weight of neat CS, the weight of grafted CS derivative and the weight of the added monomer, respectively.

2.3. Characterization of CS-MTAC

2.3.1. Nuclear magnetic resonance (NMR)

NMR spectra of CS-MTAC derivatives were obtained with an Agilent 500 spectrometer (Agilent Technologies, Santa Clara, CA, USA) operating at a frequency of 500 MHz for ^1H NMR. Deuterated acetic acid solution (2% v/v) was used as a solvent in order to prepare solutions of 5% weight/volume and the spectra were internally referenced to the solvent's residual peak.

2.3.2. Fourier-transformed Infrared spectroscopy (FT-IR)

The chemical structure of the synthesized materials was evaluated with the use of FT-IR spectroscopy. FT-IR spectra of the samples were received with an FT-IR spectrometer (FTIR-2000, Perkin Elmer, Dresden, Germany) using KBr disks (thickness of 500 μm). The spectra were collected in the range from 4000 to 400 cm^{-1} at a resolution of 2 cm^{-1} (64 co-added scans). The spectra presented are baseline corrected and converted to the absorbance mode.

2.3.3. Wide angle X-ray scattering (XRD)

X-ray powder diffraction (XRD) patterns were recorded using an XRD diffractometer (Rigaku-Minflex II) with a CuK_α radiation for crystalline phase identification ($\lambda = 0.15405 \text{ nm}$ for CuK_α). The samples were scanned from 5° to 50° and the scanning speed was $1^\circ/\text{min}$.

2.3.4. Swelling capacity

The swelling ability was evaluated by measuring the water sorption capacity at Simulated Body Fluids (SBF) buffer (pH = 7.4) [30]. Swelling studies were performed for neat CS and CS-MTAC derivative. Each sponge was carefully weighed (W_0) and was then immersed in water for several time points. At predetermined time intervals (5, 10, 15, 20, 30, 40, 50, 60, 75, 90, 120, 150 min and 24h) the sponges were retrieved from the water, the excess surface water was removed with filter paper, and the materials were weighed again in order to determine the swelling weight (W_n). The percent weight change of the samples during the swelling experiment (i.e., the cumulative weight changes due to matrix swelling and erosion). All the experiments were performed in triplicate. The $S(\text{time})\%$ was calculated using Eq. 3.

$$S(\text{time})\% = \frac{[(W_n - W_0)]}{W_0} \times 100 \quad (3)$$

2.3.5. Equilibrium water sorption/desorption isotherms (ESI/EDI)

The hydration behavior of the samples was assessed employing the technique of equilibrium water sorption/desorption isotherms (ESI/EDI) [31] at room temperature. The isothermal sorption/desorption curves were determined at room temperature by exposing the samples to fixed water vapor atmospheres in sealed jars. The relative humidity, rh , or else, water activity, was achieved with appropriate binary saturated aqueous solutions [32]. The samples were equilibrated for 7 days over relative humidity (rh) of 2, 11, 19, 33, 43, 54, 64, 75, 85, 95, and 98%. The attainment of equilibrium was determined via recording of sample weight ($m_{\text{hydrated, sample}}$). Measurements were performed simultaneously for three samples of the same type of material and results are presented here on average over these three samples. A high-accuracy Mettler Toledo balance was employed for these measurements (sensitivity of 10^{-5} g). The weights of samples after equilibration over P_2O_5 ($rh \sim 2\%$) were considered as weights in dry state ($m_{\text{dry, sample}}$).

Once the equilibrium was attained, the hydration (water content), h_d , was calculated on a dry basis through Eq. 4. The uncertainty for h values, δh , was estimated to be $\sim 0.005 \text{ wt}\%$. The hydration levels and mechanism in hydrogels, can be seen in Figure 1.

$$h_d = \frac{m_{\text{water}}}{m_{\text{dry, sample}}} = \frac{m_{\text{hydrated, sample}} - m_{\text{dry, sample}}}{m_{\text{dry, sample}}} \quad (4)$$

2.3.6. Cell viability

MTT (Sigma-Aldrich, Saint Louis, MO, USA) assay was performed 24h after the initial coating of adipose derived mesenchymal stem cells in 24-well plates, to assess the cytotoxicity of materials. Briefly, after supernatant removal from the wells, MTT reagent was added at a ratio 1:10 in DMEM medium followed by 4h incubation (37°C , 5% CO_2). The MTT was removed and 1 mL/well of dimethyl sulfoxide (DMSO) was added for one more hour for incubation under the same conditions. Absorbance was measured at 570 nm and 630 nm using a UV-Vis spectrophotometer (Perkin Elmer, Dresden, Germany). All the experiments were performed in triplicate.

The student's t test, paired with two tailed was applied to determine the effect of the chitosan modification. The difference between the results of the chitosan and modified chitosan was considered statistically significant for $p < 0.05$.

2.3.7. In vitro antibacterial activity testing

The antibacterial activity of neat CS and the synthesized CS-MTAC derivative (in 0.5% v/v acetic acid solution) was evaluated using the agar diffusion method. The bacteria studied were the Gram-negative *Escherichia coli* (ATCC 25922) and the Gram-positive *Staphylococcus aureus* (ATCC 25923). Prior

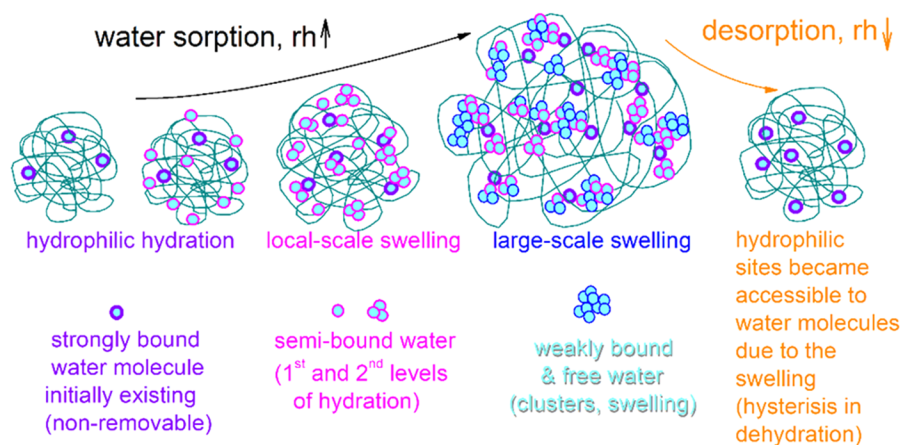


Figure 1. Schematic illustration of the mechanism of hydration levels in hydrophilic polymers (e.g., hydrogels).

Table 1. Abbreviations of hydrogels according to their chitosan, elastin, collagen, and gelatin content.

Samples	CS-MTAC (% w/v)	Elastin (% w/w)	Collagen (% w/w)	Gelatin (% w/v)
CSMTACELCG0.25 (S1)	6	4	4	0.25
CSMTACELCG0.5 (S2)	6	4	4	0.5
CSMTACELCG1 (S3)	6	4	4	1
CSMTACELCG2 (S4)	6	4	4	2

to inoculation, strains were subcultured into fresh LB at 1:50 and incubated for 2 h at 37°C, 70 rpm. Bacteria were collected by centrifugation (2300 rpm, 7 min) and resuspended in phosphate buffered saline (PBS). The number of bacteria was spectrophotometrically adjusted to O.D.600nm = 0.5 (equivalent to 1.5×10^8 CFUs/mL) and confirmed by culturing 1/10 serial dilutions of the initial suspension. Ampicillin was used as control for *Staphylococcus aureus* (*S. aureus*) and Penicillin for *Escherichia Coli* (*E. coli*). Prepared materials consisting of CS and CS-MTAC were placed into the wells and the plates were incubated for 18–24 h, at 37°C. Finally, the diameter of inhibition zones was measured as indication of antibacterial activity. All experiments were performed in triplicate.

2.4. Preparation of CS-MTAC/elastin/collagen/gelatin hydrogels

For the preparation of CS-MTAC/elastin/collagen/gelatin hydrogels, initially gelatin was added in aqueous solution under magnetic stirring for 30 min at 50°C. Subsequently, EL was dispersed under continuous magnetic stirring in GEL aqueous solution at room temperature and collagen was added after putting the solution in an ice bath. Any remaining insoluble residues were removed via centrifugation. Finally, CS powder was added before the dropwise addition of acetic acid (final amount 2% v/v) in the solution, forming a hydrogel. The obtained hydrogel was magnetically stirred until complete homogenization. The compositions of the hydrogels are shown in the following table (Table 1).

2.5. Characterization of CSMTACELCG hydrogels

2.5.1. Viscosity measurements

The rheology measurements were applied using a rheometer HAAKE™ MARS™, Thermo Fisher Scientific, USA with a

parallel plate geometry (P35/Ti, Thermo Fischer Scientific, USA) of 35 mm diameter. The measurements were performed in triplicate, at room temperature, anticipating the temperature employed for the printing process. The shear rate was recorded from 0.01 to 700 s⁻¹, the resulting curves were fitted with the Ostwald-de Waele viscosity model to determine the shear-thinning coefficient (*n*); Eq. 5.

$$\eta = K\dot{\gamma}^{n-1} \quad (5)$$

where *n* represents the power-law index and *K* the consistency index.

The amplitude sweep was conducted at 10 rad s⁻¹, to obtain the linear viscoelastic region (LVR); while the frequency sweep was conducted in the range 0.1 to 600 rad s⁻¹ to evaluate the viscoelastic properties. Finally, the three-interval thixotropy test was performed: a low shear rate of 1 s⁻¹ was applied for 30 s, followed by an increase to 100 s⁻¹ for 50 s and back to 1 s⁻¹ for 250 s.

2.5.2. Uniformity factor

The uniformity factor (*U*) was used to determine how uniform the printed strands are in comparison to the designed .STL file (doi: 10.1039/D1SM00604E). For each hydrogel sample, one fiber of 10 mm length was printed at the minimum extrusion pressure and speed of 5 mm/s and the diameter of the printed wet fiber was measured. The uniformity factor of each sample was calculated according to Eq. 6.

$$U = \frac{\text{diameter of printed strand}}{\text{diameter of theoretical straight strand}} \quad (6)$$

2.6. Fabrication of 3D printed CSELCG1 scaffolds

A Standard Tessellation Language (.STL) file of a mesh scaffold model was utilized for the 3DP of the prepared CSELCG hydrogels, while the slicing of the .STL sample was performed with Slic3r software (Figure 2). For the printability study, the scaffolds were designed as cubic mesh scaffolds (30mm length \times 30mm width \times 2.46mm height) with different infill density 40% and number of 6 layers, with angle of layers 90°. The scaffolds were fabricated with a pneumatic extrusion-based 3D Bioprinter (CELLINK® Inkredible, Gothenburg, Sweden) with needle nozzle with inner diameter of 0.41mm (G22) printing speed of 10mm/s, printing temperature of 25°C and the required minimum pressure to extrude a continuous strut for each hydrogel. In case of the final optimized scaffold the pressure was defined at 200kPa. After printing, the CSMTACELCG scaffolds were neutralized using NaOH/EtOH (NE) or ammonia vapors (N) for a period of 60 min.

For the manufacturing of the scaffolds, the resulting hydrogels were loaded into a sterile printing cartridge of 10ml and were centrifuged at 4,000rpm for 20min at 25°C to remove the air bubbles generated while stirring. When homogenous gels were formed, they were poured into the jet dispenser's nozzle syringes for 3DP process.

2.7. Characterization of 3DP scaffolds

2.7.1. Attenuated total reflectance (ATR)

Infrared (IR) spectra were recorded with a Cary 670, Agilent Technologies, equipped a diamond Attenuated Total Reflectance accessory, ATR, model Gladi ATR, Pike Technologies. Each spectrum was recorded in the range 4000–400 cm^{-1} at a resolution of 4 cm^{-1} and 32 scans after background correction.

2.7.2. Wide angle X-ray scattering (XRD)

X-ray powder diffraction (XRD) patterns were recorded using an XRD diffractometer (Rigaku-Minflex II) with a CuK_α radiation for crystalline phase identification ($\lambda=0,15405$ nm for CuK_α). The samples were scanned from 5° to 50°.

2.7.3. Swelling capacity

The swelling ability of the 3DP-S3 sample was performed as mentioned in section 2.3.4 in SBF buffer at time points 5 min, 10 min, 20 min, 30 min, 1 h, 2 h, 3 h, and 48 h.

2.7.4. Enzymatic hydrolysis

The enzymatic hydrolysis of the optimized 3DP samples was evaluated by placing it in 5 mL of SBF, pH= 7.4, containing 1 mL of a lysozyme solution (0.8 mg/mL). The sample was then inserted into an oven at 37°C and at predetermined time points (0h, 24h, 48h, 72h, 96h, 144h, and 240h), washed with distilled water, vacuum-dried in an oven at 50°C and weighted. The measurements were performed in triplicate.

2.7.5. Drug content determination and *in vitro* drug release studies

Levo was analyzed using a Shimadzu HPLC (Kyoto, Japan) system consisting of a degasser (DGU-20A5, Kyoto, Japan), a liquid chromatograph (LC-20 AD, Kyoto, Japan), an autosampler (SIL-20AC, Kyoto, Japan), a UV/Vis detector (SPD-20A, Kyoto, Japan), and a column oven (CTO-20AC, Kyoto, Japan). The column used was a type of CNW Technologies Athena C18, 120 A, 5 μm , 250 mm \times 4.6 mm set at room temperature. For the determination of the drug loading capacity of the 3D printed patches, 10 mg of the prepared levo-loaded patches were dissolved in 10 ml of

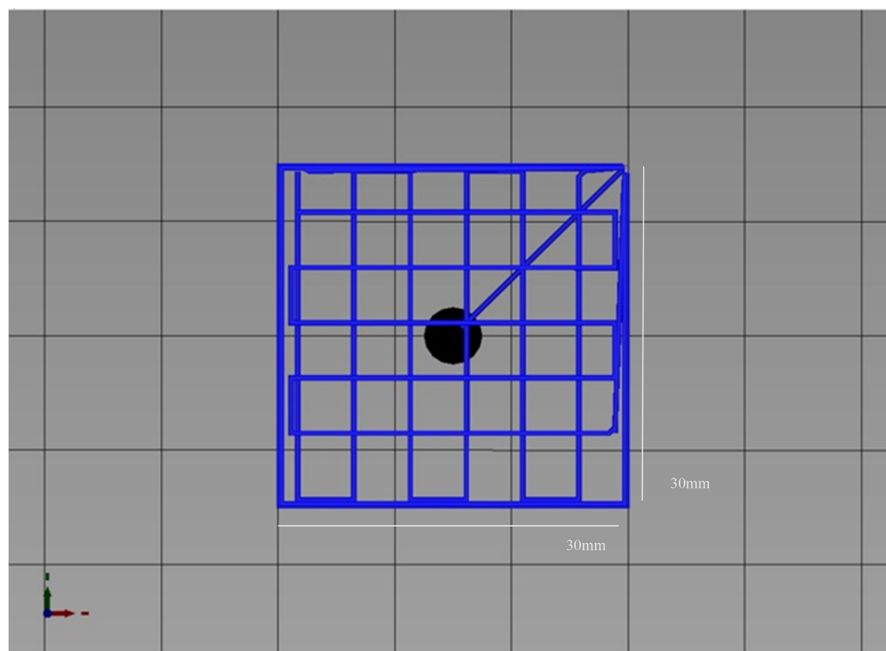


Figure 2. Computer-aided design (CAD) model of the printed construct after slicing with Slic3r.

aqueous acetic acid solution (1% v/v): methanol (60/40 v/v) [33]. The subsequent solution was stirred for 24 h and filtered through nylon filters (0.45 nm pore size). The percentage of drug loading was calculated using Eq. 7.

$$DL(\%) = \left(\frac{\text{weight of drug in patches}}{\text{weight of patches}} \right) \times 100 \quad (7)$$

For the *in vitro* release studies a dissolution apparatus type DISTEK Dissolution Apparatus Evolution 4300, equipped with an autosampler using the paddle method (USP II method), was used. Each scaffold (30 mm × 30 mm × 2.46 mm) was placed to individual dissolution vessels corresponding to 100 mg of Levo in appropriate transdermal patch holders. The test was performed at 37 ± 1 °C with a rotation speed of 100 rpm. The dissolution medium was 500 mL of a simulated body fluid, pH = 7.4 solution.

3. Results and discussion

3.1. Characterization of CS-MTAC copolymer

Chitosan grafted derivatives using acrylate or methacrylate monomers by radical polymerization, provide a promising strategy to modify the CS backbone and acquire biocompatible copolymers with new improved properties. According to the literature, radical polymerization has been initiated by persulfate ions [34,35], γ -ray irradiation [36] or metal ions [37], amongst others. In the current study, ammonium persulfate was opted as a free radical initiator, being accessible, easy-to-use and water-soluble. Besides that, this option avoids the use of metal ions since the material is intended for biomedical applications. The resulted graft CS-MTAC copolymer after radical polymerization of MTAC in the presence of CS, is illustrated in Figure 3.

Initially, the grafting percentage (GP) and grafting efficiency (GE) of the CS-MTAC derivative were calculated according to Eqs. 1 and 2, respectively. The GP corresponds to the increase of the weight of CS grafted with the MTAC monomer while the GE indicates the fraction of monomers of the CS backbone in the total polymer that have been grafted with MTAC. The GE percentage was 74% while the GP was 36%.

¹H NMR spectroscopy was used for the confirmation of the successful grafting of 2-(methacryloyloxy)ethyl trimethyl ammonium chloride (MTAC) monomer on the CS backbone (Figure 4). We can note the characteristic resonance signals due to the chitosan backbone at 3.1 ppm and the overlapping peaks at 3.7–3.9 ppm. In addition, we can observe new peaks due to the modification. The resonance signal at 1 ppm is related to the methyl group of MTAC backbone (-CH₂-C(CH₃)). Subsequently, the peak at 2 ppm includes the methylene group -CH₂-C(CH₃), with the residual acetylated CS units and the peak due to deuterated acetic acid. The peak at 3.25 ppm correspond to the methyl groups attached to the quaternary ammonium group of the copolymer (⁺N(CH₃)₃). The signals at 3.6–3.9 ppm correspond to chitosan CH and CH₂ groups as well as the CH₂ groups from MTAC, which confirms the graft of the monomer to the chitosan. The intense peaks at 4.78 ppm and near 2 ppm in all spectra are attributed to residual solvent peaks.

To further confirm the successful grafting of MTAC onto CS, FTIR spectra of neat CS, MTAC and the graft copolymer were also recorded (Figure 5). As can be seen, the main characteristic bands of CS are presented. The broad overlapped peak at 3000–3600 cm⁻¹ is assigned to the vibrations of -OH and N-H bonds. The bands at 1653 cm⁻¹ and 1597 cm⁻¹ are attributed to amide I (>C=O stretching) and amide II (N-H bending), respectively. Furthermore, peaks at 1423 cm⁻¹ (C-H and O-H vibrations), 1379 cm⁻¹ (C-N axial deformation), 1154 cm⁻¹ (anti-symmetric stretching of the C-O-C bridge) and 1084 cm⁻¹ (C-O stretching vibrations) can be shown. Furthermore, in both unmodified and modified chitosan polymers, adsorption bands at 893, 942, and 1109 cm⁻¹ are attributed to C-O ring stretching, CH₃ bending vibration, and C-O-C stretching, respectively. With regard to MTAC monomer, the typical peak at 1716 cm⁻¹ is due to stretching vibrations of the carbonyl group and the bands at 1488 and 957 cm⁻¹ are attributed to the bending and stretching vibrations of the quaternary ammonium group (-N(CH₃)₃), respectively. Regarding CS-MTAC copolymer, a light shift of the peaks of hydroxyl groups of neat CS from 3426 cm⁻¹ to 3408 cm⁻¹ and free amino groups from 2877 cm⁻¹ to 2906 cm⁻¹ is noticed due to hydrogen bonds between chitosan and MTAC. The C=O stretching band of MTAC is appeared in the derivative at 1723 cm⁻¹

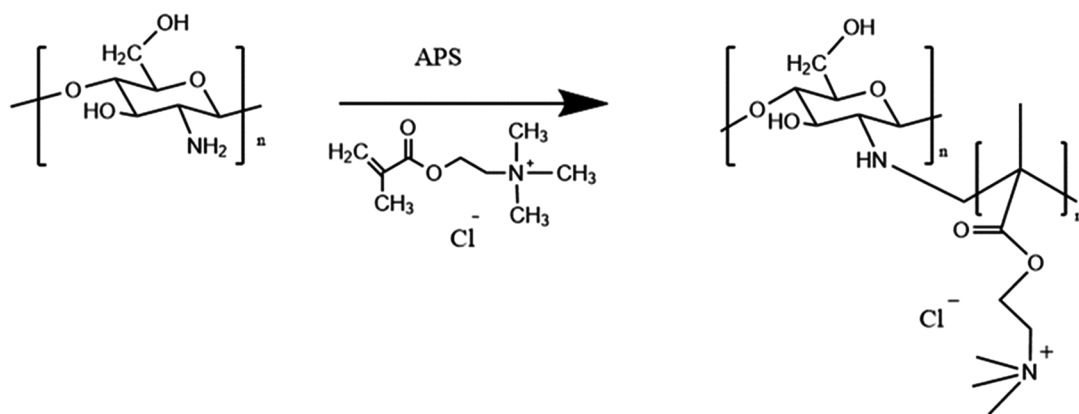


Figure 3. Schematic illustration of CS-MTAC grafting reaction.

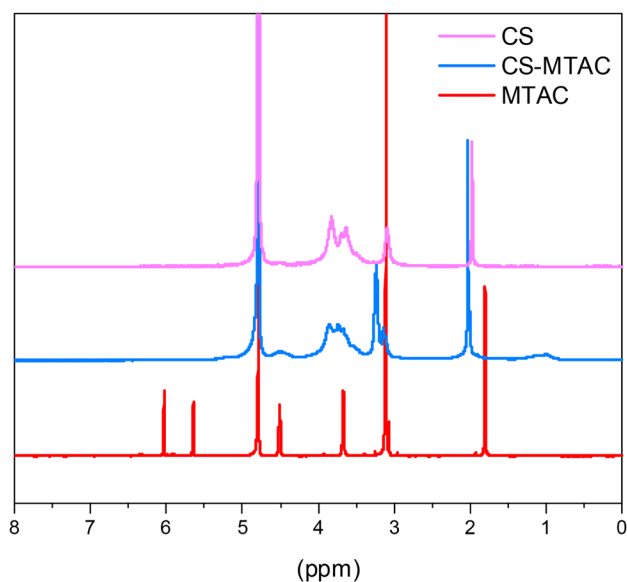


Figure 4. ^1H NMR spectra of CS, MTAC and CS-MTAC.

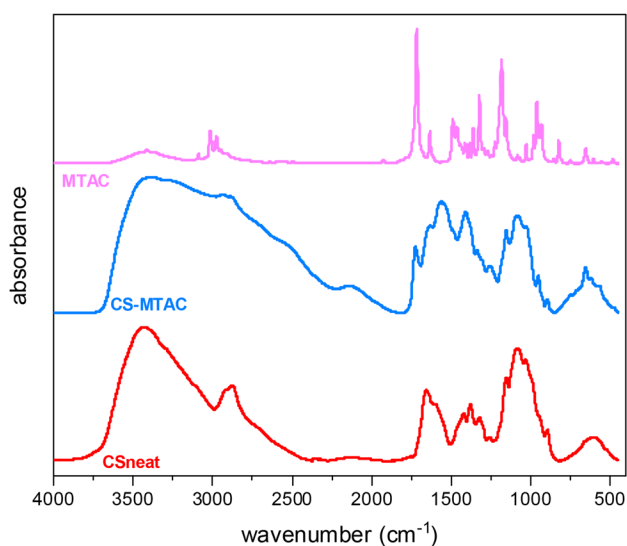


Figure 5. FTIR spectra of CS, MTAC and CS-MTAC.

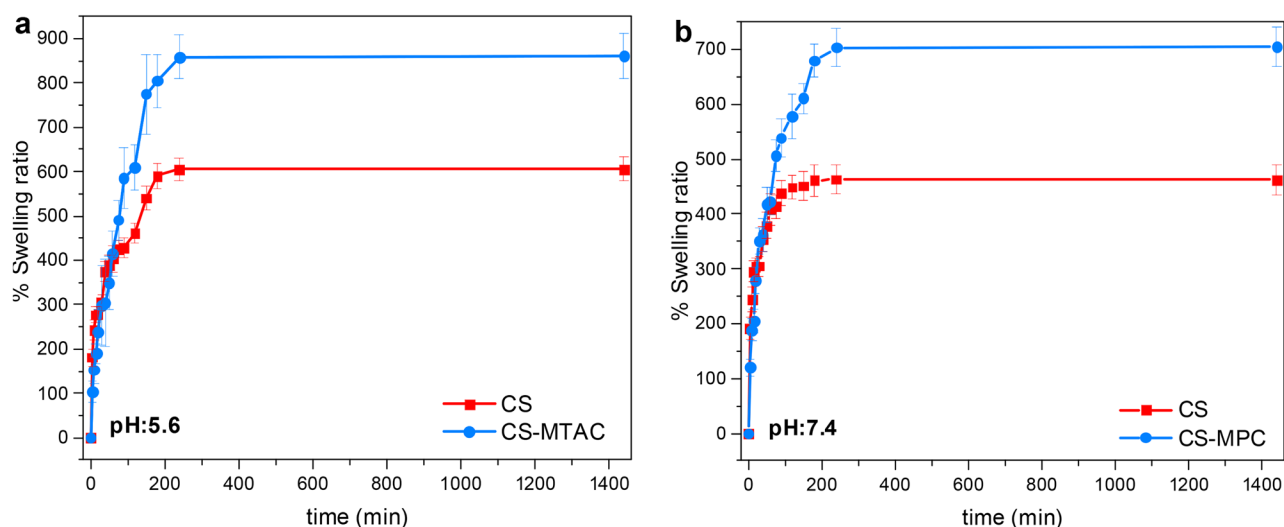


Figure 6. Degree of swelling of CS-MTAC derivative as a function of time at (a) pH 5.6 and (b) pH 7.4.

and the peak at 957 cm^{-1} is coming from the $-\text{N}(\text{CH}_3)_3$ group. All these FTIR findings provide further evidence for the successful grafting of MTAC onto CS macromolecular chain.

The crystallinity of CS-MTAC compared to neat CS was examined with XRD measurements (Figure S1) The XRD pattern for chitosan powder reveals a strong peak of 20.1° and one weak peak of 9° at 2θ , which are the indicators of the existence of crystalline and amorphous regions, respectively. The diminished intensity of the CS-MTAC diffractogram compared to the initial polysaccharide is ascribed to the insertion of MTAC, which is a small molecule and reduce the ability of CS-MTAC to fold and acquire a crystalline structure. However, the prepared CS-MTAC derivative is also a semicrystalline polymer having two distinct peaks at 9.25° and 20.28° , which indicates that has a similar crystalline structure with neat CS.

The chemical structure of the polymer could have an impact on the swelling ratio of the hydrogels. As a result, hydrogels containing hydrophilic groups swell to a higher degree compared to those containing hydrophobic groups. Since swelling is strongly related to the drug release behavior, the swelling capacity was studied in phosphate buffer saline (PBS) at pH 7.4, since is the medium where in the drug release experiments took part [38]. In addition, the value of pH 5.6 was selected as a way to simulate the pH of a non-infected wound [39]. Consequently, the swelling property of CS-MTAC derivative, compared to neat CS, was studied in two pH (5.6 and 7.4) and the degree of swelling is presented in Figure 6.

For both values of pH, the degree of swelling for neat CS increased rapidly within the first 20 min followed by a stabilization, which is typical behavior for CS [40]. Concerning CS-MTAC, the tertiary amino group included in MTAC provides an increase to the hydrophilicity of neat chitosan that is obvious in both pH studied. Specifically, at pH 5.6, the swelling percentage for CS-MTAC was 860% and for neat CS 589% while at pH 7.4 was 710% and 462% respectively. It is perceived that the degree of

swelling decreases with increasing pH, thereby showing pH-responsive swelling behavior. At a lower pH (pH 5.6), protonation of the amino groups of CS takes place, which causes electrostatic force of repulsion among intra- and inter-polymeric chains [41]. As a result, the polymeric network becomes loose which leads to an enhancement in water absorption. However, at a higher pH (pH: 7.4), the amine group is not ionized and interact with each other through hydrogen bonds [42], which decreases the swelling percentage. This property may contribute to eliminating the wound exudates timely [43].

Figure 7 presents the water content measured on dry sample basis, h_d , as a function of the rh for the neat chitosan, CS. Based on the result for the h_d (rh) pattern, we conclude that the h_d pattern belongs to the Class II according to the Brunauer classification [44], which is the expected trend for CS [29,45].

For the low rh , the water uptake is low and mild, as the initial water molecules entering the sample are few and are attached on initial hydrophilic sites (1st and 2nd hydration levels, Figure 7). For neat CS, these correspond to the h_d increasing from 0 up to 0.25 wt. For the higher $rh > 65\%$, the recorded change from linear behavior to a strong water uptake is rationalized in terms of the formation of water clusters. The latter is facilitated by the simultaneous softening of the polymer matrix and the overall sample's swelling (plasticization). The maximum water uptake of neat CS is estimated at $h_d \sim 0.50$ wt for rh of 98%.

Coming to the effect of the MTAC, we observe in Figure 7b that the 1st and 2nd hydration levels are somehow suppressed. This could suggest that a small fraction of the initial hydration sites is either decreased or are not accessible by the water molecules. However, owing to the high-water uptakes and the swelling properties at the higher rh are comparable for both the modified samples have not become more rigid, so the second case is excluded.

The maximum water uptakes are the same for CS-MTAC as compared to neat CS (Figure 8). Respectively, this suggests that at the highest water activity, the modified samples

exhibit similar and higher ability of swelling, despite the more complex chitosan structure. This is very promising in case of the use of the material in the moist environment of a wound as it can allow the delivery of topical treatments such as antimicrobials or analgesics and at the same time promote the wound healing process through circulation of the epithelial cells, avoiding the formation of eschar [46].

With the purpose of confirming the viability and cytocompatibility of fibroblasts cells upon exposure to the materials, the new CS-MTAC derivatives were tested with an MTT assay (Figure 9b). According to previous studies, the used acrylate monomer showed no cytotoxicity [27]. The results of the MTT assay on cell proliferation on prepared material in comparison with the neat chitosan are presented in Figure 9a. Since reduction of MTT can only occur in metabolically active cells, the level of activity is a measure of the viability of the cells. The synthesized materials exhibit satisfactory biocompatibility after 24h of the test and viable cells are still detected after 72h of exposure. Similar results were also reported by Yu et al. who prepared the CS with Poly[2-(methacryloyloxy)ethyl] trimethyl ammonium chloride (PMETAC) hydrogel as a wound dressing. Interestingly, according to this research, polyMETAC alone was slightly cytotoxic [27]. Statistical analysis revealed no significant difference between chitosan and chitosan derivative. As a consequence, the biocompatibility of the new copolymer further supported its potential as effective vehicle for wound healing applications.

The antimicrobial behavior of the chitosan derivative CS-MTAC was studied against *S. aureus* and *E. coli* and the different inhibition zones observed are presented in Table 2. Neat CS exhibits already some activity against *S. aureus* and *E. coli*. This result is in accordance with the literature data where CS is one of the most important polymers with inherent antibacterial properties [47]. It was found that chitosan can bind the outer membranes of several bacteria, due to the evolved interactions between the negatively charged surface of microbial cell membranes and the positively charged amino groups of the structure of CS [9,48]. The antibacterial

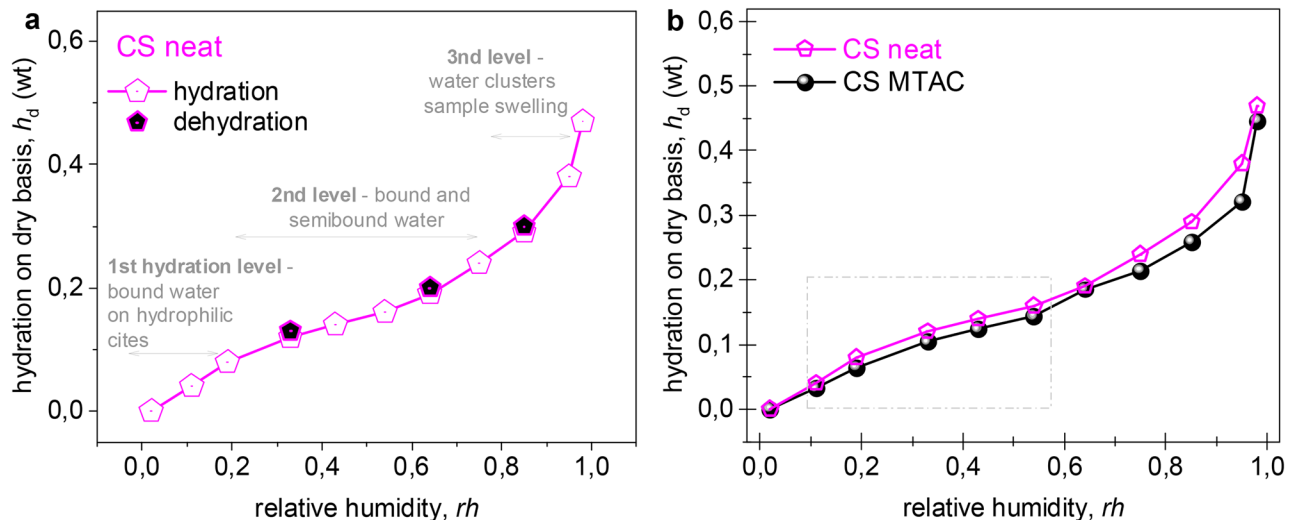


Figure 7. The water content or else hydration on dry basis, h_d , against relative humidity during the ESI/DSI measurements of (a) neat CS and (b) CS-MTAC compared to neat CS.

activity of MTAC has been reported in recently work [49,50]. The grafting of CS with MTAC resulted in additional positively charged groups that were introduced on the CS backbone. Accordingly, it is expected that the CS-MTAC derivative will reveal stronger antibacterial properties compared to neat CS. As indicated, prepared copolymer appeared larger inhibition zone than neat CS. Moreover, it is noticed that the antibacterial activity of CS-MTAC against *E. coli* was better than *S. Aureus*.

3.2. Characterization of CS-MTAC/elastin/collagen/gelatin hydrogels

CS-based hydrogels are attractive candidates to produce bio-inks. However, given the poor rheological properties of CS, finding an appropriate gelling agent is fundamental to meet the requirements for 3DP (e.g., shear-thinning behavior, good recovery rate). For this purpose, EL-COL and increasing concentrations of GEL were incorporated into the formulation. The shear rate test, frequency sweep and recovery test were performed to evaluate the printability

performance, thus select the optimal formulation to print the final design.

The flow curves, represented in Figure 11a, show that all formulations presented a non-Newtonian behavior, characterized by a decrease in the viscosity values with increasing shear rate. Upon the action of the shear stress, the decrease in the viscosity is attributable to the disentanglement of the polymer networks of the hydrogel [51]. The Ostwald-de Waele model (Eq. 5) was applied to obtain additional information concerning the shear thinning behavior and the consistency of the formulations. The fitted parameters are reported in Table 3. Overall, all formulations possessed $n < 1$, demonstrating the shear thinning behavior, a fundamental prerequisite for a successful printing process. Furthermore, the effect of increasing concentration of GEL on the consistency of the hydrogel was observed, confirming the thickening effect.

In addition, after the identification of the linear viscoelastic region (LVR) through the amplitude sweep test (data not shown), the viscoelastic properties of the formulations were investigated through the frequency sweep test. This test allows predicting the flow through the nozzle and the structural stability of the printed design. For this purpose, the storage modulus (G') and loss modulus (G'') were determined, where G' typically represents the elastic behavior, while G'' is associated with the viscous behavior. As depicted in Figure 10b, for each formulation, both moduli increased with increasing angular frequency (ω). Specifically, S1, S2, and S3 possessed $G'' > G'$ at low frequency, showing the predominance of the viscous behavior that might be related to the entanglement network between the hydrogel components. Followed by a faster increase of the elastic modulus at higher frequencies, specifically for S2 and S3, indicating a shift to a solid-like behavior. For the above-mentioned formulations, the relaxation time (τ) was calculated from the reciprocal crossover frequency and reported in Table 3. For S1, the differences between the storage and loss moduli, at low frequency, are greater than the other formulations. Moreover, the relaxation time is lower (0.16s), suggesting poor shape fidelity after printing. On the contrary, S4

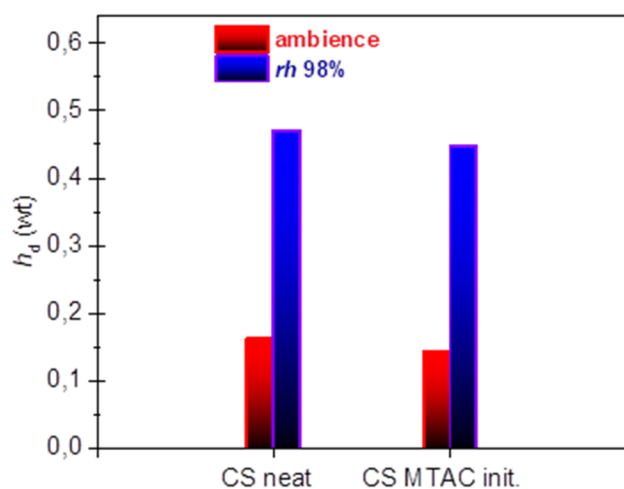


Figure 8. The h_d values for ambient conditions and at the maximum rh measured.

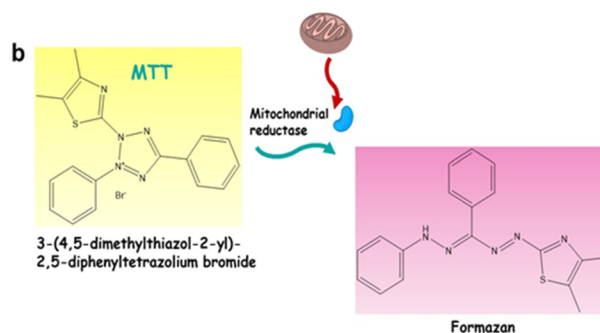
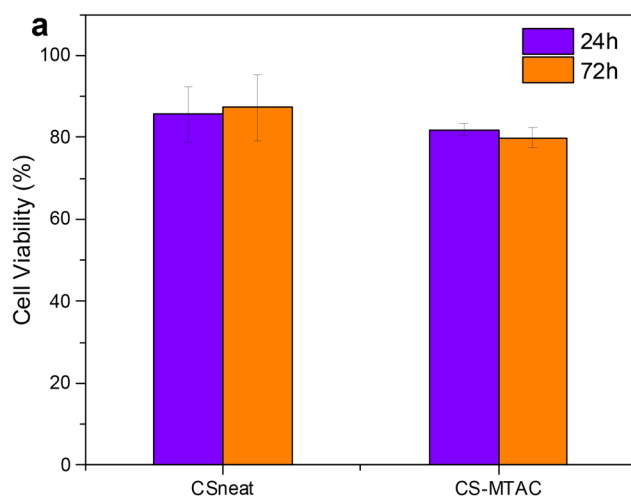


Figure 9. (a) MTT assays results on the proliferation of fibroblasts exposed to the scaffolds, (b) schematic illustration of MTT assay.

presented $G' > G''$ over the entire ω range, demonstrating a solid-like behavior, attributable to the higher concentration of GEL that, by nature, possesses solid-like properties [52]. However, this behavior might lead to poor printability performances.

Finally, the thixotropic behavior of the formulations was investigated over time. For this purpose, the changes in the viscosity were analyzed as a function of three shear intervals that mimic the different stages of the printing process. Firstly, a low shear stress is applied representing the resting condition before printing, followed by an increase in the shear values mimicking the flow of the hydrogel through the nozzle. Then, the shear values increase representing the recovery after extrusion. The recovery rate obtained was compared at 100s and reported in Table 3. S4 showed the lowest recovery rate (28.67%), while for the other formulations the values slightly differ. Nevertheless, the highest recovery rate was obtained from the formulation S3 (66.91%).

Overall, considering the optimal results achieved through the full rheological characterization (shear thinning behavior, optimal relaxation time and good recovery rate), S2 and S3 were selected as potential candidates to print the design. To further evaluate the printability performance the uniformity factor was investigated (Figure S2).

S3 sample showed the best printing behavior among the hydrogels, as the U factor was almost equal to 1 at all conditions, producing smooth and uniform filaments. The results of U for S2 and S3 using G22 nozzle at 25°C are presented in Figure S3. The macroscopic image of the 3DP scaffolds prepared, is shown in Figure 11.

The addition of a strong NaOH (1M) solution to the printed structures leads to the augmentation of the pH value reaching the alkali region, where CS-MTAC is insoluble. The increase in the pH above 6.5 leads to a sol-gel transition of the CS-MTAC-based hydrogel, forming a three-dimensional network due to the generation of physical junctions of H bonds which promote the packing of the macromolecular chains. The primary amino groups are neutralized, forming extensive hydrophobic interactions and hydrogen bonds among the different moieties present in the CS-MTAC and GEL backbones, such as amino, hydroxyl, and carbonyl groups. In the case of NaOH/EtOH neutralization agent there is a better stability and integrity of the shape

compared to NH_3 vapors as long as is a stronger base ($\text{pH}_{\text{NaOH/EtOH}} = 12.55$, $\text{pH}_{\text{NH}_3} = 9.3$). It is noted that the use of NH_3 vapors leads to decreased crosslinking density and forming a quite loose network.

3.3. Characterization of 3DP-S3 scaffolds

From FTIR spectra (Figure 12), EL appears two main peaks at 1530cm^{-1} and 1658cm^{-1} that corresponded to the amide II and amide I bonds, respectively [53]. Indeed, these peaks overlapped with the corresponding peaks of amide II and amide I in chitosan at 1560cm^{-1} and 1636cm^{-1} , respectively [54]. In the spectrum of COL, the main absorption bands that correspond to amide I, amide II, and amide III appear at 1634 , 1524 , and 1164cm^{-1} , respectively. The broad band at $3000\text{--}3700\text{cm}^{-1}$ attributes to the N-H stretching vibration of amide I and the asymmetrical C-H stretching vibrations of amide II [55]. Following, ATR of GEL appears the characteristic peak at 1239cm^{-1} corresponding to C-N, N-H vibrations in amide III, while the peaks at 1532cm^{-1} , 1632cm^{-1} and 3280cm^{-1} are the peaks referring to C=O and, N-H vibrations in amide I and O-H stretching vibration, respectively [56]. Checking the differences between the spectra of the neat materials and the one obtained from the blend, some shifts were detected. Spectrum of CSMTACELCG1 was observed to present a shift of the carbonyl groups shifted from 1628cm^{-1} to 1640cm^{-1} , and the amino groups shifted from 1565cm^{-1} to 1537cm^{-1} . Adding, the characteristic peak at 3252cm^{-1} of the hydroxyl groups we can confirm the hydrogen bond between carboxyl, amino and hydroxyl moieties of the ingredients of the formulation.

Figure 12b illustrates the ATR spectrum of 3DP S3 scaffold before and after neutralization. In general, it was noticed that the characteristic peaks of 3DP S3 are affected after gelation. Particularly, both neutralized scaffolds with NaOH/EtOH (3DP-S3-NE) and ammonia vapors (3DP-S3-N) exhibit a lower intensity peak of the amide II band at 1540cm^{-1} than non-neutralized. Furthermore, this peak is lower in the samples that were neutralized with NaOH/EtOH than the neutralized with ammonia vapors. This may happen due to the neutralization of free NH_3^+ groups of CS into NH_2 groups. In general, peak broadening is observed in the spectra of the cross-linked scaffolds. In particular, the characteristic absorption at 1538cm^{-1} is shifted, exhibiting a lower intensity peak, due to N-H bending vibrations [57], due to the removal of acetic acid residues [58]. Also, low-intensity sharp peaks are recorded in the neutralized samples at $\sim 1400\text{cm}^{-1}$, which corresponds to the bending of $-\text{CH}_2-$ [59].

Concerning the components of the scaffold, the diffraction patterns of pure GEL are the typical amorphous pattern

Table 2. Inhibition growth zones of CS and its CS-MTAC derivatives against the studied strains.

	Area of inhibition (diameter mm)	
	E. coli (Gram -)	S.aureus (Gram +)
Gentamycin-control	12 ± 2	Ampicillin-control 25 ± 2
CS	5 ± 1	CS 4 ± 0.5
CS-MTAC	7 ± 0.6	CS-MTAC 5 ± 0.8

Table 3. Rheological parameters of Ostwald-de Waele model (n , K , r^2), relaxation time (τ) and recovery rate obtained from each formulation.

Sample	n	K	r^2	τ (s)	Recovery Rate (%)
S1	0.48 ± 0.01	59.98 ± 3.13	0.9987 ± 0.0001	0.16 ± 0.02	66.29 ± 1.02
S2	0.44 ± 0.01	107.35 ± 0.65	0.9987 ± 0	1.56 ± 0.01	64.89 ± 0.15
S3	0.46 ± 0.01	74.48 ± 0.31	0.9991 ± 0.0001	0.39 ± 0.02	66.91% ± 0.22
S4	0.42 ± 0.01	125.95 ± 0.75	0.9994 ± 0	–	28.67 % ± 0.12

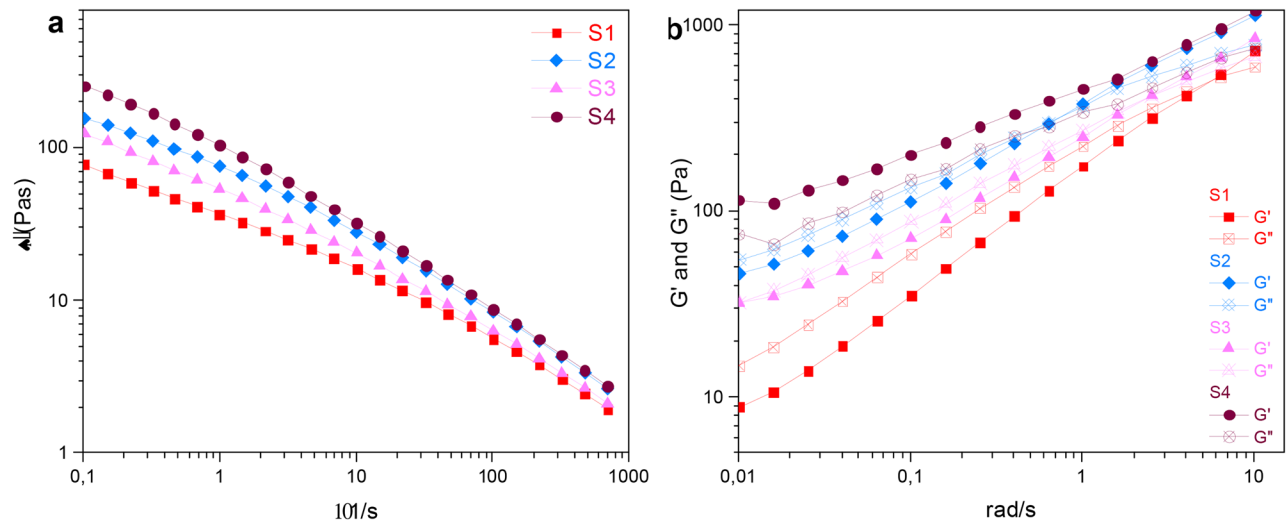


Figure 10. (a) Shear rate test and (b) Frequency sweep test of S1, S2, S3, S4 formulations. Where G' is represented as solid, while G'' allow symbols.

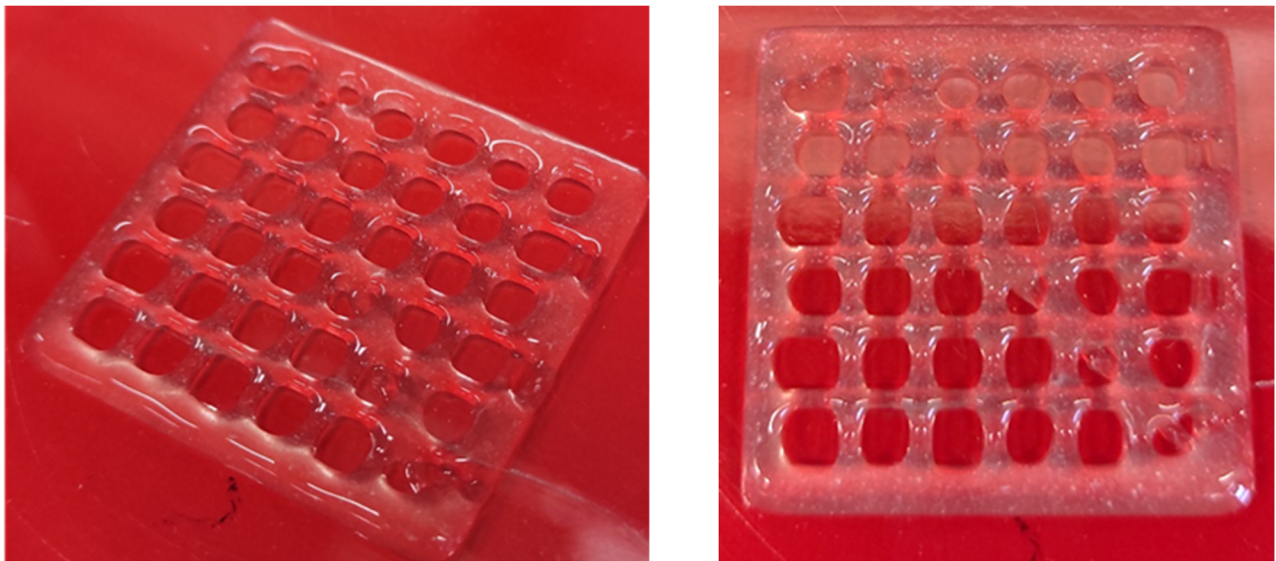


Figure 11. 3DP multilayered (6 layers) scaffold of CSMTACELCG1 (S3), printed at room temperature, before gelation.

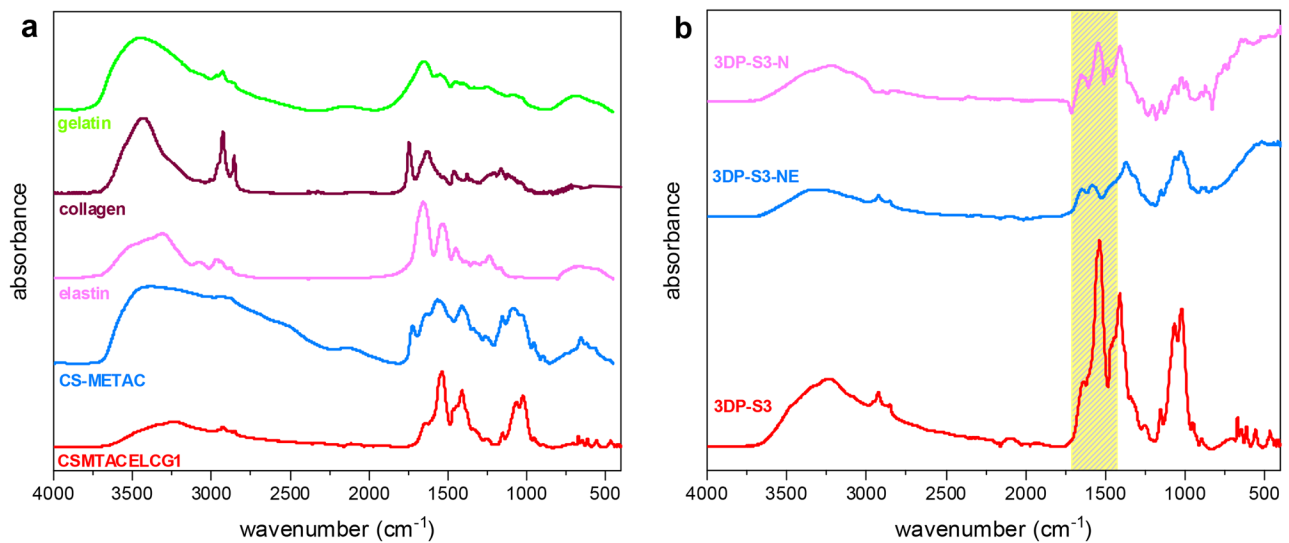


Figure 12. FTIR spectra of (a) 3DP-S3 and its components CS-MTAC, EL, COL and GEL and (b) 3DP-S3 before and after neutralization with NE and N.

of proteins with a broad peak at 20° related to its semi-crystalline nature originating from α -helix and triple-helical structure [60]. The diffraction spectra of pure type I COL show a peak at 8° corresponding to the intermolecular side deposition of the COL chains in the triple helices and a broad peak at $20\sim 20^\circ$, which is attributed to the location of the characteristic voids between the peptide chains in the triple helices [61]. The broad peak of the EL XRD pattern at $\sim 20^\circ$ supports the suggestion that is closely related to COL in its structure, being also a protein.

Moreover, the neutralization of the samples with NaOH has an impact on their crystalline structure. The sol-gel transition occurring during gelation provokes a reorganization of the polymeric chains, leading to changes in the crystalline structure of the 3DP-S3 structures. The characteristic diffraction peaks of chitosan are broadened and shifted while the characteristic halo pattern is captured with reduced intensity. This observation is in accordance with the bibliography where, the mixing of proteins with chitosan leads to a

decrease in crystallinity, which is ascribed to hydrogen bonds and enhances their good compatibility [62]. Also, Takara *et al.*, reported, that a differentiation in CS semicrystalline peaks when treated with different NaOH solutions [63] (Figure 13).

3.4. Characterization of loaded 3DP-S3 scaffolds

For the study of the successful loading of levo in the S3 samples and the determination of the potential interactions between the drug and polymeric matrixes, FTIR measurements were performed (Figure 14). As mentioned in the literature, levo appears its principal peaks at $3177\text{--}3327\text{ cm}^{-1}$ due to the hydroxyl groups of $-\text{COOH}$, at $2793\text{--}2949\text{ cm}^{-1}$ due to aromatic group stretching, at 1718 cm^{-1} due to stretching of the carbonyl group and at 1287 cm^{-1} due to stretching of amines (C-N). The peak at 1084 cm^{-1} is correlated to the presence of C-halogen group, while the N-H bending vibrations in the quinolone molecule are recorded

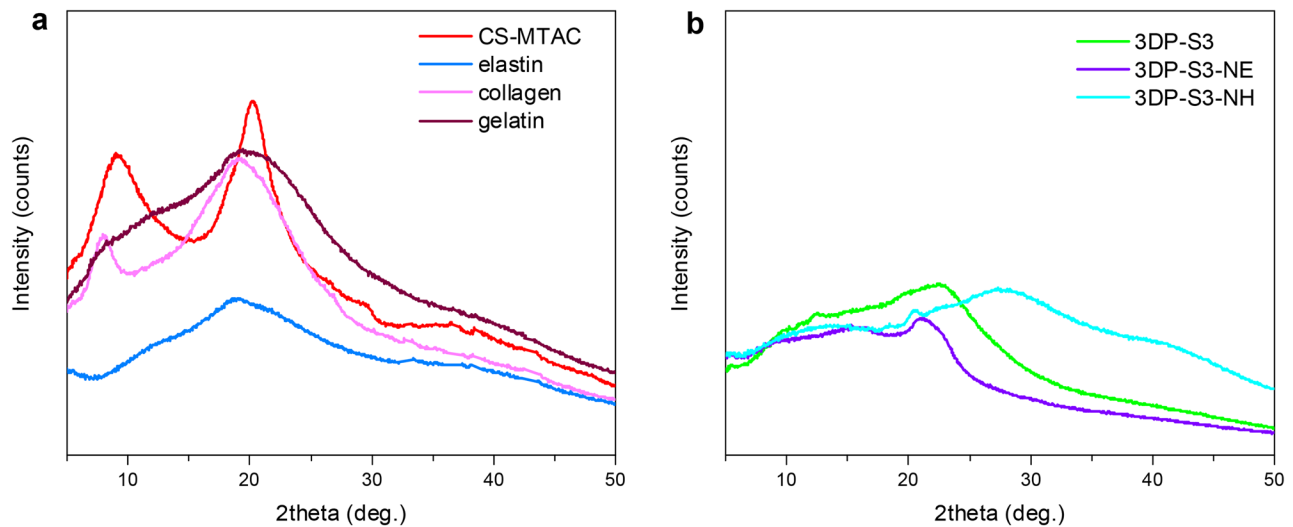


Figure 13. X-ray diffractograms of (a) CS-MTAC, EL, COL, GEL, and (b) 3DP-S3 before and after neutralization with NE and N.

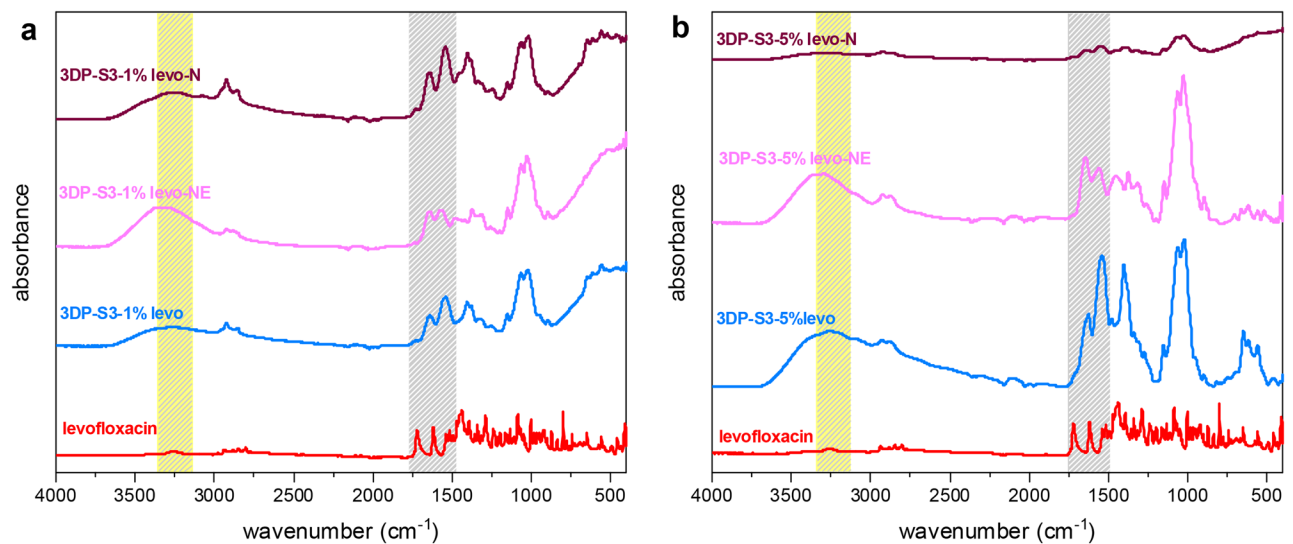


Figure 14. IR spectra of 3DP-S3 loaded sample with (a) 1% and (b) 5% of levofloxacin neutralized with NaOH/EtOH and ammonia vapors.

at 1613 cm^{-1} . Regarding the spectra of the loaded S3 sample, the carbonyl groups are recorded at region $1726\text{--}1741\text{ cm}^{-1}$ while the N-H vibrations in the quinolone molecule are reported at 1643 cm^{-1} . In addition, the hydroxyl group area is recorded at $3265\text{--}3292\text{ cm}^{-1}$, respectively at 3432 cm^{-1} in neat S3. These shifts indicate the formation of hydrogen bonds between levo and the polymeric matrix [33]. Concerning the NE-treated samples we observe the strong absorption peaks at 3288 and 3377 cm^{-1} , attributed to the stretching of the amino and hydroxyl groups in both concentration of levo [33]. N-treated samples were shown similar spectra to the untreated sample. The differences observed among the scaffolds could be attributed to the different distribution of water molecules occurring during the polysaccharide neutralization process.

Levo is a crystalline compound as confirmed by the crystallography data with sharp characteristic diffraction peaks recorded in the angle range of $5\text{--}50^\circ$ (Figure 15) [64]. In the loaded samples the halo structures are preserved, which is expected in compliance with the literature data. It is observed that for the 1% loaded sample, the halo structure is preserved, as well as a broadening at the peaks at 9° and 15° . The neutralizing process of 3DPS3 with NaOH/EtOH and NH_3 vapors cause a general reduction of the crystallinity of the sample. This decrease is directly connected with the loss of hydrogen bonding and deprotonation of the amino groups of CS after neutralization. Concerning the 1% loaded sample, the non-neutralized sample is amorphous presenting some peaks of low intensity coming from levo (9.3° , 15.2° and 22°). In the case of 5% loaded sample, no certain peak is recorded probably due to amorphization of the drug as extensive hydrogen bonding of the drug with the CS-MTAC was developed. A reduction of the peak at 12.47° which is attributed to the hydrated polymorph of chitosan is obvious in all neutralized samples [65]. This is connected to decrease of hydrogen bonding and deprotonation of the amino groups of chitosan during neutralization. Interestingly, ammonia vapors triggered crystallization into the anhydrous form in both concentrations of levo, promoting interchain hydrogen

bonds in the crystalline regions without the presence of water molecules [66].

DSC measurements (Figure S4) were performed to further confirm the XRD results. Levo, as a crystalline compound, presents a melting peak at 237°C . Moreover, CS is a polysaccharide with a characteristic endothermic peak at $60\text{--}100^\circ\text{C}$, coming from its loss of moisture and exothermic peak at 295°C , when the decomposition of the polymeric matrix occurs [67,68]. None of the samples revealed the characteristic endothermic peak of levo while the decomposition of polysaccharides occurred. These results confirmed the amorphous loading of levo into the 3DP structures. Remarkably, there is a decrease in the peak around 100°C of the untreated and neutralized samples with NE and N. This may happen because of the unbound water is trapped during gelation process. Furthermore, the peak is more intense in the case of NE than N, because it promotes stronger gelation suggesting that there is a correlation between gelation conditions and the amount of bulk water in the samples [69].

One crucial property of the polymeric materials designed for dermal patches is their ability to swell in aqueous environments. Figure 16 presents the swelling ability and enzymatic hydrolysis of the 3DP-S3. Our formulation has the potential to absorb the 214% of its dry mass. In particular, the swelling process follows a two-phase behavior an initial fast swelling phase during the first 1h followed by a small increment and a steady swelling phase. It worth mentioning that the swelling efficiency was lower in the printed samples in comparison to the initial CS-MTAC material, which is attributed to the different form of tested materials, sponges, and films, respectively. The swelling property is very useful for wound healing applications as the dressing should absorb any exudates of the wound while providing a physiologically moist environment to provide protection against bacterial infection [70]. Subsequently, the enzymatic hydrolysis of the 3DP sample causes gradually the depolymerization of CS-MTAC via the scission of the sensitive $\beta\text{-}1,4$ glycosidic bond [71]. The mass loss during enzymatic hydrolysis among

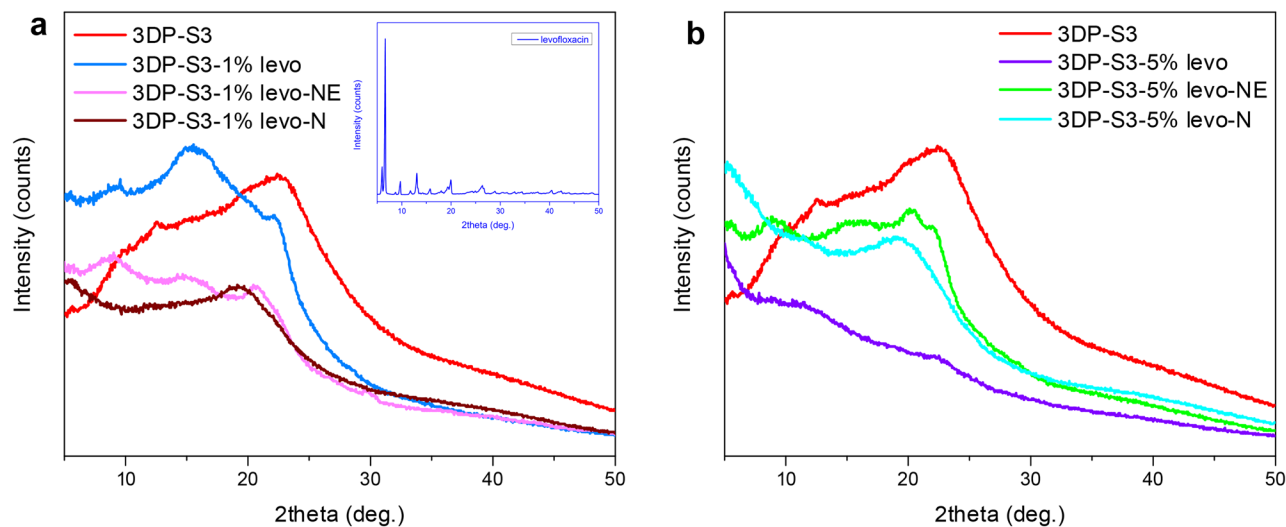


Figure 15. XRD diffractograms of 3DP-S3 loaded sample with (a) 1% and (b) 5% of levofloxacin neutralized with NaOH/EtOH and ammonia vapors.

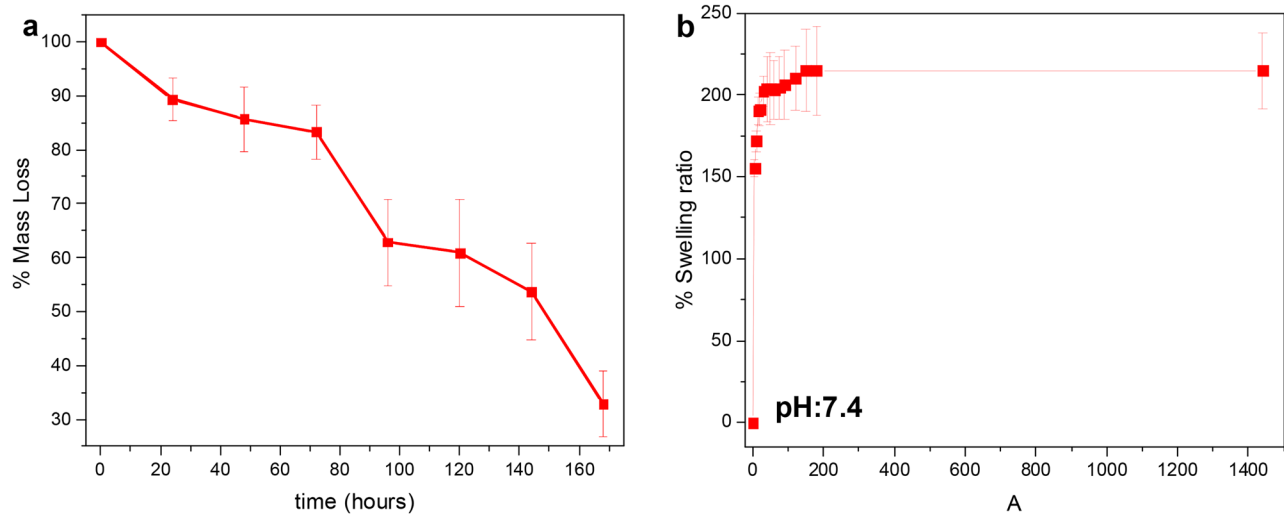


Figure 16. (a) Enzymatic hydrolysis and (b) degree of swelling of 3DP-S3 wound dressing.

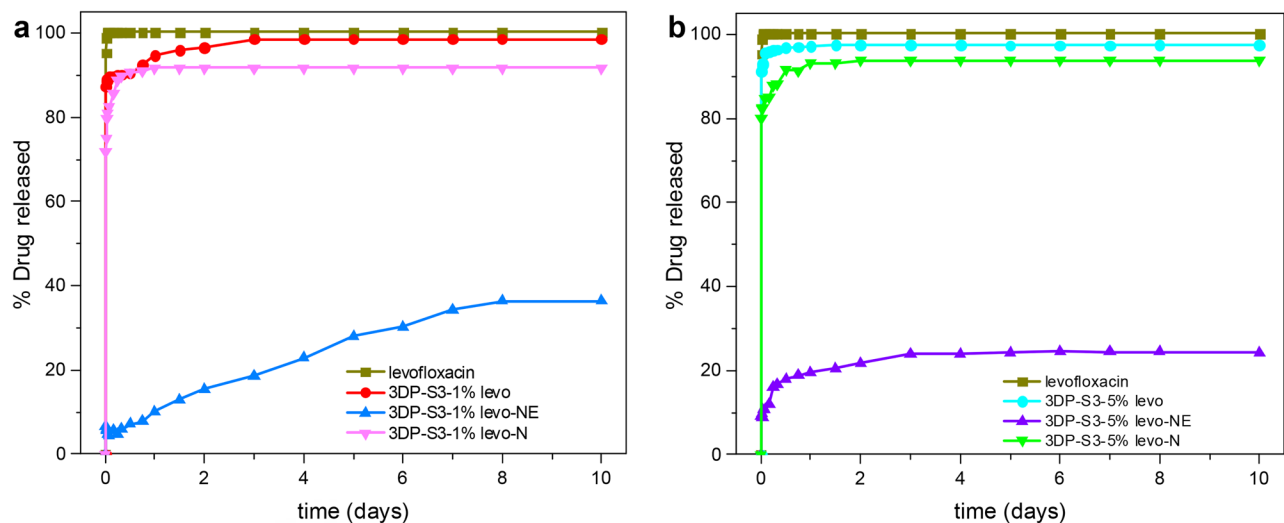


Figure 17. *In-vitro* release of levo from 3DP-S3, 3DP-S3-NE, 3DP-S3-N with levo concentration of (a) 1% and (b) 5% w/w.

others depends on the swelling behavior. The relative low swelling capacity leads to insufficient distribution of the enzyme into the polymeric chains, resulting to lower degradation of the bonds referred.

The drug loading results indicated satisfying values, specifically 0.6% for the samples theoretically containing 1% of levo and 4.13% for the samples with theoretically 5%. *In vitro* dissolution studies were conducted for the evaluation of levo release rate. Figure 17 shows the dissolution profiles of neat levo and 3DP S3 scaffolds loaded with 1% and 5% w/w of levo.

Almost all formulations, except of those treated with NE, showed an initial burst release approximately the first 6h, followed by a subsequent sustained release of 10 days of the dissolution process, reaching 90-98%. This is very important as this release can inhibit microbial growth in an open wound, promoting the wound healing process.

Due to the thermosensitive nature of prepared scaffolds, the raised temperature (37°C) leads to the partial breakage of hydrogen bonds between CS-MTAC and GEL resulting in the sectional dissolution of the S3 hydrogel matrix [72,73]. In

addition, the prepared scaffolds swell in pH 7.4 buffer, allowing water molecules to easily enter the hydrogel network and cause larger and faster degradation, thus enhancing drug release capacity [74]. Notably, from the S3 non-neutralized patches the water-soluble levo is released in a percentage > 80% from the first hour of control and almost completely (>95%) in both concentrations after 24h when a fully swollen hydrogel has been formed (Figure S4). Consequently, sufficient control of the drug release is not achieved.

The scaffolds treated with ammonia vapors show a rapid release of the drug during the first hour leading to a lower quantity (approximately 85%) due to the limited swelling capacity compared to non-neutralized samples. S3-NE in both concentrations of the drug, 1% and 5% w/w, has been observed to release smaller amounts of levo, 36% and 24%, respectively with a slower release rate. This is due to the strong interactions that occur during the neutralization process. These interactions and the formation of dense structures reduce the swelling capacity and degradation rate,

resulting in decreased drug release [66]. Additionally, the lower dissolution rate of 3DP-S3-NE-5% levo compared to the lower concentration may occur due its slightly lower crystallinity.[75] In general, the mechanism of drug release from matrices containing swellable polymers is complex enough and not fully understood. A diffusion or erosion mechanism is observed, while most systems reveal a combination of these mechanisms. As a result, the levofloxacin release is probably controlled initially by the swelling ability of the matrix and by diffusion at the extended periods of release [76].

The retention of the structure after the release of the neutralized samples is a result of the formation of hydrogen bonds between the neutralization agent and the hydrogel (Figure S5). Additionally, the gelation reaction in ammonia vapors is milder compared to NaOH/EtOH, probably allowing a local rearrangement of polymeric chains of chitosan as the gelation agent penetrates the scaffold, resulting in a higher tendency for water absorption [69].

4. Conclusions and future directions

In the present study, the structure of CS was successfully modified with MTAC as proved by NMR and FTIR measurements. The synthesized copolymer exhibited enhanced swelling ability in both pH 5.6 and 7.4 while for low hydration levels the introduction of MTAC seems to hinder the water molecules to access the initial hydrophilic sites of the material. The new antibacterial material was blended with elastin, collagen, and gelatin and were investigated for their ability to be 3DP in an extrusion printer for first time. As most polymeric hydrogel inks are not self-standing and are prone to collapse or spread after printing due to gravitational forces, post-printing procedure was followed using NaOH/EtOH and NH_3^+ vapors as neutralizing agents in order to improve the stability. The optimized formulation was used to be loaded with levo antibiotic drug, envisaged for wound healing applications. Furthermore, FTIR measurements confirmed the successful loading of levo into the 3D-printed samples, whereas XRD and DSC measurements established the amorphous state of levo encapsulated in the mixture. The *in vitro* release studies indicated the enhanced release of levo in the dissolution medium and reached 98% during the 10 days process. It seems that the option of NaOH/EtOH as a crosslinking agent is promising since it results to stable structures even after the release process and could be an alternative to the conventional use of other crosslinkers of chitosan like dialdehydes (e.g., glutaraldehyde) or tripolyphosphate, diglycidyl ether, ethylene glycol and toluene-2,4-diisocyanate which presents cytotoxicity and biocompatibility issues [74,77]. The aforementioned results render the 3D-printed CS-MTAC/EL/COL/GEL loaded with levo systems potential candidates for the treatment of several skin infections.

Future directions could include testing the 3D printed formulations on experimental skin in order to check the diffusion of the antibiotic in the local site and also the regeneration process in the direction of a step closer to the market of these kind of constructs. Nevertheless, the absence of

certain regulatory about these constructs preventing the transition from research to clinic should be underlined. Therefore, the development of protocols for full scale production strategies should become a priority.

Acknowledgements

Authors would like to thank Eleni Gounari and Biohellenika S.A for cytotoxicity and antibacterial properties measurements.

Declaration of interest

All parties confirm there was no conflict of interest.

CRedit authorship contribution statement

Maria Lazaridou: Methodology, Investigation, Formal Analysis, Writing – original draft, Writing – review and editing. **Sofia Moroni:** Methodology, Formal analysis, Writing – review and editing. **Panagiotis Klonos:** Investigation. **Apostolos Kyritsis:** Writing – review & editing. **Dimitrios N. Bikiaris:** Supervision, Writing – review & editing. **Dimitrios A. Lamprou:** Supervision, Conceptualization, Methodology, Writing – review & editing.

Data availability statement

The data that support the findings of this study are available from the corresponding author upon reasonable request.

References

- [1] Bowler, P. G.; Duerden, B. I.; Armstrong, D. G. Wound Microbiology and Associated Approaches to Wound Management. *Clin. Microbiol. Rev.* 2001, 14, 244–269. DOI: 10.1128/CMR.14.2.244-269.2001.
- [2] Liu, H.; Wang, C.; Li, C.; Qin, Y.; Wang, Z.; Yang, F.; Li, Z.; Wang, J. A Functional Chitosan-Based Hydrogel as a Wound Dressing and Drug Delivery System in the Treatment of Wound Healing. *RSC Adv.* 2018, 8, 7533–7549. DOI: 10.1039/c7ra13510f.
- [3] Stewart, M. W.; Stewart, M. W. Current Treatment Recommendations. *Diabetic Retinopathy.* 2017, 57, 163–186. DOI: 10.1007/978-981-10-3509-8_6.
- [4] Sargur Ranganath, A.; Jemina, M.; Nagaraju, N.; Hashimoto, M. Evaluating 3D-Printability of Polyvinyl Alcohol (PVA) and Microfibrillated Cellulose (MFC) Composite Inks. *Mater. Today Proc.* 2022, 70, 6–11. DOI: 10.1016/j.matpr.2022.08.483.
- [5] Di Luca, M.; Hoskins, C.; Corduas, F.; Onchuru, R.; Oluwasanmi, A.; Mariotti, D.; Conti, B.; Lamprou, D. A. 3D Printed Biodegradable Multifunctional Implants for Effective Breast Cancer Treatment. *Int. J. Pharm.* 2022, 629, 122363. DOI: 10.1016/j.ijpharm.2022.122363.
- [6] Alonso-Fernández, I.; Haugen, H. J.; López-Peña, M.; González-Cantalapiedra, A.; Muñoz, F. Use of 3D-Printed Polylactic Acid/Bioceramic Composite Scaffolds for Bone Tissue Engineering in Preclinical in Vivo Studies: A Systematic Review. *Acta Biomater.* 2023, 168, 1–21. DOI: 10.1016/j.actbio.2023.07.013.
- [7] Lackner, F.; Knechtel, I.; Novak, M.; Nagaraj, C.; Dobaj Štiglic, A.; Kargl, R.; Olschewski, A.; Stana Kleinschek, K.; Mohan, T. 3D-Printed Anisotropic Nanofiber Composites with Gradual Mechanical Properties. *Adv. Mater. Technol.* 2023, 8, 2201708. DOI: 10.1002/admt.202201708.
- [8] Lazaridou, M.; Bikiaris, D. N.; Lamprou, D. A. 3D Bioprinted Chitosan-Based Hydrogel Scaffolds in Tissue Engineering and

- Localised Drug Delivery. *Pharmaceutics*. 2022, 14, 1978. DOI: [10.3390/pharmaceutics14091978](https://doi.org/10.3390/pharmaceutics14091978).
- [9] Zamboulis, A.; Nanaki, S.; Michailidou, G.; Koumentakou, I.; Lazaridou, M.; Ainali, N. M.; Xanthopoulou, E.; Bikiaris, D. N. Chitosan and Its Derivatives for Ocular Delivery Formulations: Recent Advances and Developments. *Polymers (Basel)*. 2020, 12, 1519. DOI: [10.3390/polym12071519](https://doi.org/10.3390/polym12071519).
- [10] Sousa, C. F. V.; Monteiro, L. P. G.; Rodrigues, J. M. M.; Borges, J.; Mano, J. F. Marine-Origin Polysaccharides-Based Free-Standing Multilayered Membranes as Sustainable Nanoreservoirs for Controlled Drug Delivery. *J. Mater. Chem. B*. 2023, 11, 6671–6684. DOI: [10.1039/d3tb00796k](https://doi.org/10.1039/d3tb00796k).
- [11] Yilmaz Atay, H. Antibacterial Activity of Chitosan-Based Systems. In *Functional Chitosan*; Springer Singapore: Singapore, 2019; pp 457–489. DOI: [10.1007/978-981-15-0263-7_15](https://doi.org/10.1007/978-981-15-0263-7_15).
- [12] Khan, A.; Alamry, K. A. Recent Advances of Emerging Green Chitosan-Based Biomaterials with Potential Biomedical Applications: A Review. *Carbohydr. Res.* 2021, 506, 108368. DOI: [10.1016/j.carres.2021.108368](https://doi.org/10.1016/j.carres.2021.108368).
- [13] Ouro, P. M. S.; Costa, D. C. S.; Amaral, A. J. R.; Mano, J. F. A Supramolecular Injectable Methacryloyl Chitosan-Tricine-Based Hydrogel with 3D Printing Potential for Tissue Engineering Applications. *Macromol. Biosci.* 2023, 24, e2300058. DOI: [10.1002/mabi.202300058](https://doi.org/10.1002/mabi.202300058).
- [14] Jurko, L.; Makuc, D.; Štern, A.; Plavec, J.; Žegura, B.; Bošković, P.; Kargl, R. Cytotoxicity and Antibacterial Efficacy of Betaine- and Choline-Substituted Polymers. *ACS Appl. Polym. Mater.* 2023, 5, 5270–5279. DOI: [10.1021/acsapm.3c00691](https://doi.org/10.1021/acsapm.3c00691).
- [15] Carmona-Ribeiro, A.; de Melo Carrasco, L. Cationic Antimicrobial Polymers and Their Assemblies. *Int. J. Mol. Sci.* 2013, 14, 9906–9946. DOI: [10.3390/ijms14059906](https://doi.org/10.3390/ijms14059906).
- [16] Davidenko, N.; Schuster, F.; Bax, V. D.; Farndale, R. W.; Hamaia, S.; Best, M. S.; Cameron, E. R. Evaluation of Cell Binding to Collagen and Gelatin: A Study of Theeffect of 2D and 3D Architecture and Surface Chemistry. *Journal of Materials Science: Materials in Medicine*. 2016, 27(148), 539–547.
- [17] Liu, J. C.; Heilshorn, S. C.; Tirrell, D. A. Comparative Endothelial Cell Response to Artificial Extracellular Matrix Proteins Containing the RGD and CS5 Cell-Binding Domains. *Biomacromolecules*. 2004, 5, 497–504. DOI: [10.1021/bm034340z](https://doi.org/10.1021/bm034340z).
- [18] Magli, S.; Rossi, G. B.; Risi, G.; Bertini, S.; Cosentino, C.; Crippa, L.; Ballarini, E.; Cavaletti, G.; Piazza, L.; Masseroni, E.; et al. Design and Synthesis of Chitosan–Gelatin Hybrid Hydrogels for 3D Printable in Vitro Models. *Front. Chem.* 2020, 8, 524. DOI: [10.3389/fchem.2020.00524](https://doi.org/10.3389/fchem.2020.00524).
- [19] Kim, E. H.; Lim, S.; Kim, T. E.; Jeon, I. O.; Choi, Y. S. Preparation of in Situ Injectable Chitosan/Gelatin Hydrogel Using an Acid-Tolerant Tyrosinase. *Biotechnol. Bioproc. E.* 2018, 23, 500–506. DOI: [10.1007/s12257-018-0315-4](https://doi.org/10.1007/s12257-018-0315-4).
- [20] Kristensen, J. H.; Karsdal, M. A. Elastin. In *Biochemistry of Collagens, Laminins and Elastin: Structure, Function and Biomarkers*; Elsevier Inc., 2016; pp 197–201. DOI: [10.1016/B978-0-12-809847-9.00030-1](https://doi.org/10.1016/B978-0-12-809847-9.00030-1).
- [21] Wen, Q.; Mithieux, S. M.; Weiss, A. S. Elastin Biomaterials in Dermal Repair. *Trends Biotechnol.* 2020, 38, 280–291. DOI: [10.1016/j.tibtech.2019.08.005](https://doi.org/10.1016/j.tibtech.2019.08.005).
- [22] Mela, P.; Hinderer, S.; Kandail, H. S.; Bouten, C. V. C.; Smits, A. I. P. M. Tissue-Engineered Heart Valves. In *Principles of Heart Valve Engineering*; Elsevier, 2019; pp 123–176. DOI: [10.1016/B978-0-12-814661-3.00006-X](https://doi.org/10.1016/B978-0-12-814661-3.00006-X).
- [23] Posniak, S.; Chung, J. H. Y.; Liu, X.; Mukherjee, P.; Wallace, G. G. The Importance of Elastin and Its Role in Auricular Cartilage Tissue Engineering. *Bioprinting*. 2023, 32, e00276. DOI: [10.1016/j.bprint.2023.e00276](https://doi.org/10.1016/j.bprint.2023.e00276).
- [24] Perez-puyana, V.; Villanueva, P.; Jiménez-rosado, M.; de la Portilla, F.; Romero, A. Incorporation of Elastin to Improve Polycaprolactone-Based Scaffolds for Skeletal Muscle via Electrospinning. *Polymers (Basel)*. 2021, 13, 1501. DOI: [10.3390/polym13091501](https://doi.org/10.3390/polym13091501).
- [25] Grover, C. N.; Cameron, R. E.; Best, S. M. Investigating the Morphological, Mechanical and Degradation Properties of Scaffolds Comprising Collagen, Gelatin and Elastin for Use in Soft Tissue Engineering. *J. Mech. Behav. Biomed. Mater.* 2012, 10, 62–74. DOI: [10.1016/j.jmbbm.2012.02.028](https://doi.org/10.1016/j.jmbbm.2012.02.028).
- [26] Gaspar-Pintilie, A.; Stanciu, A. M.; Craciunescu, O. Natural Composite Dressings Based on Collagen, Gelatin and Plant Bioactive Compounds for Wound Healing: A Review. *Int. J. Biol. Macromol.* 2019, 138, 854–865. DOI: [10.1016/j.ijbiomac.2019.07.155](https://doi.org/10.1016/j.ijbiomac.2019.07.155).
- [27] Yu, Q.; Yan, Y.; Huang, J.; Liang, Q.; Li, J.; Wang, B.; Ma, B.; Bianco, A.; Ge, S.; Shao, J. A Multifunctional Chitosan-Based Hydrogel with Self-Healing, Antibacterial, and Immunomodulatory Effects as Wound Dressing. *Int. J. Biol. Macromol.* 2023, 231, 123149. DOI: [10.1016/j.ijbiomac.2023.123149](https://doi.org/10.1016/j.ijbiomac.2023.123149).
- [28] Heydarifard, S.; Gao, W.; Fatehi, P. Impact of Counter Ions of Cationic Monomers on the Production and Characteristics of Chitosan-Based Hydrogel. *ACS Omega*. 2019, 4, 15087–15096. DOI: [10.1021/acsomega.9b01953](https://doi.org/10.1021/acsomega.9b01953).
- [29] Lazaridou, M.; Nanaki, S.; Zamboulis, A.; Papoulia, C.; Chrissafis, K.; Klonos, P. A.; Kyritsis, A.; Vergkizi-Nikolakaki, S.; Kostoglou, M.; Bikiaris, D. N. Super Absorbent Chitosan-Based Hydrogel Sponges as Carriers for Caspofungin Antifungal Drug. *Int. J. Pharm.* 2021, 606, 120925. DOI: [10.1016/j.ijpharm.2021.120925](https://doi.org/10.1016/j.ijpharm.2021.120925).
- [30] Wang, C. C.; Chen, C. C. Anti-Bacterial and Swelling Properties of Acrylic Acid Grafted and Collagen/Chitosan Immobilized Polypropylene Non-Woven Fabrics. *J. Appl. Polym. Sci.* 2005, 98, 391–400. DOI: [10.1002/app.22224](https://doi.org/10.1002/app.22224).
- [31] Pissis, P.; Kyritsis, A. Hydration Studies in Polymer Hydrogels. *J. Polym. Sci. B. Polym. Phys.* 2013, 51, 159–175. DOI: [10.1002/polb.23220](https://doi.org/10.1002/polb.23220).
- [32] Greenspan, L. Humidity Fixed Points of Binary Saturated Aqueous Solutions. *J. Res. Natl. Bur. Stan. Sect. A*. 1977, 81A, 89. DOI: [10.6028/jres.081A.011](https://doi.org/10.6028/jres.081A.011).
- [33] Siafaka, P. I.; Zisi, A. P.; Exindari, M. K.; Karantas, I. D.; Bikiaris, D. N. Porous Dressings of Modified Chitosan with Poly(2-Hydroxyethyl Acrylate) for Topical Wound Delivery of Levofloxacin. *Carbohydr. Polym.* 2016, 143, 90–99. DOI: [10.1016/j.carbpol.2016.02.009](https://doi.org/10.1016/j.carbpol.2016.02.009).
- [34] Filippousi, M.; Siafaka, P. I.; Amanatiadou, E. P.; Nanaki, S. G.; Nerantzaki, M.; Bikiaris, D. N.; Vizirianakis, I. S.; Van Tendeloo, G. Modified Chitosan Coated Mesoporous Strontium Hydroxyapatite Nanorods as Drug Carriers. *J. Mater. Chem. B*. 2015, 3, 5991–6000. DOI: [10.1039/c5tb00827a](https://doi.org/10.1039/c5tb00827a).
- [35] Harish Prashanth, K. V.; Tharanathan, R. N. Studies on Graft Copolymerization of Chitosan with Synthetic Monomers. *Carbohydr. Polym.* 2003, 54, 343–351. DOI: [10.1016/S0144-8617\(03\)00191-7](https://doi.org/10.1016/S0144-8617(03)00191-7).
- [36] Zhou, Y.; Hua, S.; Yu, J.; Dong, P.; Liu, F.; Hua, D. A Strategy for Effective Radioprotection by Chitosan-Based Long-Circulating Nanocarriers. *J. Mater. Chem. B*. 2015, 3, 2931–2934. DOI: [10.1039/c5tb00063g](https://doi.org/10.1039/c5tb00063g).
- [37] Zhang, J.; Yuan, Y.; Shen, J.; Lin, S. Synthesis and Characterization of Chitosan Grafted Poly(N,N-Dimethyl-N-Methacryloxyethyl-N-(3-Sulfopropyl) Ammonium) Initiated by Ceric (IV) Ion. *Eur. Polym. J.* 2003, 39, 847–850. DOI: [10.1016/S0014-3057\(02\)00286-0](https://doi.org/10.1016/S0014-3057(02)00286-0).
- [38] Peppas, N. A.; Bures, P.; Leobandung, W.; Ichikawa, H. Hydrogels in Pharmaceutical Formulations. *Eur. J. Pharm. Biopharm.* 2000, 50, 27–46. DOI: [10.1016/S0939-6411\(00\)00090-4](https://doi.org/10.1016/S0939-6411(00)00090-4).
- [39] Rahimi, R.; Ochoa, M.; Parupudi, T.; Zhao, X.; Yazdi, I. K.; Dokmeci, M. R.; Tamayol, A.; Khademhosseini, A.; Ziaie, B. A Low-Cost Flexible PH Sensor Array for Wound Assessment. *Sens. Actuators B Chem.* 2016, 229, 609–617. DOI: [10.1016/j.snb.2015.12.082](https://doi.org/10.1016/j.snb.2015.12.082).
- [40] Feng, D.; Bai, B.; Wang, H.; Suo, Y. Enhanced Mechanical Stability and Sensitive Swelling Performance of Chitosan/Yeast Hybrid Hydrogel Beads. *New J. Chem.* 2016, 40, 3350–3362. DOI: [10.1039/C5NJ02404H](https://doi.org/10.1039/C5NJ02404H).
- [41] Ng, W. L.; Yeong, W. Y.; Naing, M. W. Development of Polyelectrolyte Chitosan-Gelatin Hydrogels for Skin Bioprinting. *Procedia CIRP* 2016, 49, 105–112. DOI: [10.1016/j.procir.2015.09.002](https://doi.org/10.1016/j.procir.2015.09.002).

- [42] Choi, Y. R.; Kim, E. H.; Lim, S.; Choi, Y. S. Efficient Preparation of a Permanent Chitosan/Gelatin Hydrogel Using an Acid-Tolerant Tyrosinase. *Biochem. Eng. J.* 2018, *129*, 50–56. DOI: [10.1016/j.bej.2017.10.016](https://doi.org/10.1016/j.bej.2017.10.016).
- [43] Liang, Y.; Zhao, X.; Hu, T.; Chen, B.; Yin, Z.; Ma, P. X.; Guo, B. Adhesive Hemostatic Conducting Injectable Composite Hydrogels with Sustained Drug Release and Photothermal Antibacterial Activity to Promote Full-Thickness Skin Regeneration during Wound Healing. *Small.* 2019, *15*, e1900046. DOI: [10.1002/smll.201900046](https://doi.org/10.1002/smll.201900046).
- [44] Uni, G. W.; Brunauer, S. Der Waals Adsorption of Gases * *And1940*, 1139 (6).
- [45] Gámiz-González, M. A.; Piskin, A. E.; Pandis, C.; Chatzimanolis-Moustakas, C.; Kyritsis, A.; Mari, B.; Ribelles, J. L. G.; Vidaurre, A. Determining the Influence of N-Acylation on Water Sorption in Chitosan Films. *Carbohydr. Polym.* 2015, *133*, 110–116. DOI: [10.1016/j.carbpol.2015.07.020](https://doi.org/10.1016/j.carbpol.2015.07.020).
- [46] Nuutila, K.; Eriksson, E. Moist Wound Healing with Commonly Available Dressings. *Adv. Wound Care (New Rochelle)*. 2021, *10*, 685–698. DOI: [10.1089/wound.2020.1232](https://doi.org/10.1089/wound.2020.1232).
- [47] Yan, D.; Li, Y.; Liu, Y.; Li, N.; Zhang, X.; Yan, C. Antimicrobial Properties of Chitosan and Chitosan Derivatives in the Treatment of Enteric Infections. *Molecules*. 2021, *26*, 7136. DOI: [10.3390/molecules26237136](https://doi.org/10.3390/molecules26237136).
- [48] Helander, I. M.; Nurmiaho-Lassila, E. L.; Ahvenainen, R.; Rhoades, J.; Roller, S. Chitosan Disrupts the Barrier Properties of the Outer Membrane of Gram-Negative Bacteria. *Int. J. Food Microbiol.* 2001, *71*, 235–244. DOI: [10.1016/S0168-1605\(01\)00609-2](https://doi.org/10.1016/S0168-1605(01)00609-2).
- [49] Wang, H.; Chen, M.; Jin, C.; Niu, B.; Jiang, S.; Li, X.; Jiang, S. Antibacterial [2-(Methacryloyloxy) Ethyl] Trimethylammonium Chloride Functionalized Reduced Graphene Oxide/Poly(Ethylene-Co-Vinyl Alcohol) Multilayer Barrier Film for Food Packaging. *J. Agric. Food. Chem.* 2018, *66*, 732–739. DOI: [10.1021/acs.jafc.7b04784](https://doi.org/10.1021/acs.jafc.7b04784).
- [50] Garcia, I. M.; Rodrigues, S. B.; de Souza Balbinot, G.; Visioli, F.; Leitune, V. C. B.; Collares, F. M. Quaternary Ammonium Compound as Antimicrobial Agent in Resin-Based Sealants. *Clin. Oral Investig.* 2020, *24*, 777–784. DOI: [10.1007/s00784-019-02971-4](https://doi.org/10.1007/s00784-019-02971-4).
- [51] Rajput, I. B.; Tareen, F. K.; Khan, A. U.; Ahmed, N.; Khan, M. F. A.; Shah, K. U.; Rahdar, A.; Diez-Pascual, A. M. Fabrication and in Vitro Evaluation of Chitosan-Gelatin Based Aceclofenac Loaded Scaffold. *Int. J. Biol. Macromol.* 2023, *224*, 223–232. DOI: [10.1016/j.ijbiomac.2022.10.118](https://doi.org/10.1016/j.ijbiomac.2022.10.118).
- [52] Sonaye, S. Y.; Ertugral, E. G.; Kothapalli, C. R.; Sikder, P. Extrusion 3D (Bio)Printing of Alginate-Gelatin-Based Composite Scaffolds for Skeletal Muscle Tissue Engineering. *Materials (Basel)*. 2022, *15*, 7945. DOI: [10.3390/ma15227945](https://doi.org/10.3390/ma15227945).
- [53] Annabi, N.; Fathi, A.; Mithieux, S. M.; Martens, P.; Weiss, A. S.; Dehghani, F. The Effect of Elastin on Chondrocyte Adhesion and Proliferation on Poly (E{Open}-Caprolactone)/Elastin Composites. *Biomaterials*. 2011, *32*, 1517–1525. DOI: [10.1016/j.biomaterials.2010.10.024](https://doi.org/10.1016/j.biomaterials.2010.10.024).
- [54] Su, H.; Fujiwara, T.; Bumgardner, J. D. A Study of Combining Elastin in the Chitosan Electrospinning to Increase the Mechanical Strength and Bioactivity. *Mar. Drugs*. 2021, *19*, 169. DOI: [10.3390/MD19030169](https://doi.org/10.3390/MD19030169).
- [55] Terzopoulou, Z.; Michopoulou, A.; Palamidi, A.; Koliakou, E.; Bikiaris, D. Preparation and Evaluation of Collagen-Based Patches as Curcumin Carriers. *Polymers (Basel)*. 2020, *12*, 1–18. DOI: [10.3390/polym12102393](https://doi.org/10.3390/polym12102393).
- [56] Peng, J.; Wang, X.; Lou, T. Preparation of Chitosan/Gelatin Composite Foam with Ternary Solvents of Dioxane/Acetic Acid/Water and Its Water Absorption Capacity. *Polym. Bull.* 2020, *77*, 5227–5244. DOI: [10.1007/s00289-019-03016-2](https://doi.org/10.1007/s00289-019-03016-2).
- [57] Mauricio-Sánchez, R. A.; Salazar, R.; Luna-Bárceñas, J. G.; Mendoza-Galván, A. FTIR Spectroscopy Studies on the Spontaneous Neutralization of Chitosan Acetate Films by Moisture Conditioning. *Vib. Spectrosc.* 2018, *94*, 1–6. DOI: [10.1016/j.vibspec.2017.10.005](https://doi.org/10.1016/j.vibspec.2017.10.005).
- [58] Lagaron, J. M.; Fernandez-Saiz, P.; Ocio, M. J. Using ATR-FTIR Spectroscopy to Design Active Antimicrobial Food Packaging Structures Based on High Molecular Weight Chitosan Polysaccharide. *J. Agric. Food Chem.* 2007, *55*, 2554–2562. DOI: [10.1021/jf063110j](https://doi.org/10.1021/jf063110j).
- [59] Dong, Y.; Xu, C.; Wang, J.; Wang, M.; Wu, Y.; Ruan, Y. Determination of Degree of Substitution for N-Acylated Chitosan Using IR Spectra. *Sci. China Ser. B Chem.* 2001, *44*, 216–224. DOI: [10.1007/BF02879541](https://doi.org/10.1007/BF02879541).
- [60] Liu, F.; Antoniou, J.; Li, Y.; Ma, J.; Zhong, F. Rheological and Viscoelastic Properties of Chitosan Solutions Prepared with Different Chitosan or Acetic Acid Concentrations. *Foods*. 2015, *45*, 140–149. DOI: [10.3390/foods11172692](https://doi.org/10.3390/foods11172692).
- [61] Davidenko, N.; Schuster, C. F.; Bax, D. V.; Farndale, R. W.; Hamaia, S.; Best, S. M.; Cameron, R. E. Evaluation of Cell Binding to Collagen and Gelatin: A Study of the Effect of 2D and 3D Architecture and Surface Chemistry. *J. Mater. Sci. Mater. Med.* 2016, *27*, 148. DOI: [10.1007/s10856-016-5763-9](https://doi.org/10.1007/s10856-016-5763-9).
- [62] Zhai, M.; Zhao, L.; Yoshii, F.; Kume, T. Study on Antibacterial Starch/Chitosan Blend Film Formed under the Action of Irradiation. *Carbohydr. Polym.* 2004, *57*, 83–88. DOI: [10.1016/j.carbpol.2004.04.003](https://doi.org/10.1016/j.carbpol.2004.04.003).
- [63] Takara, E. A.; Marchese, J.; Ochoa, N. A. NaOH Treatment of Chitosan Films: Impact on Macromolecular Structure and Film Properties. *Carbohydr. Polym.* 2015, *132*, 25–30. DOI: [10.1016/j.carbpol.2015.05.077](https://doi.org/10.1016/j.carbpol.2015.05.077).
- [64] Gorman, E. M.; Samas, B.; Munson, E. J. Understanding the Dehydration of Levofloxacin Hemihydrate. *J. Pharm. Sci.* 2012, *101*, 3319–3330. DOI: [10.1002/jps.23200](https://doi.org/10.1002/jps.23200).
- [65] He, Q.; Ao, Q.; Gong, Y.; Zhang, X. Preparation of Chitosan Films Using Different Neutralizing Solutions to Improve Endothelial Cell Compatibility. *J. Mater. Sci. Mater. Med.* 2011, *22*, 2791–2802. DOI: [10.1007/s10856-011-4444-y](https://doi.org/10.1007/s10856-011-4444-y).
- [66] Becerra, J.; Sudre, G.; Royaud, I.; Montserret, R.; Verrier, B.; Rochas, C.; Delair, T.; David, L. Tuning the Hydrophilic/Hydrophobic Balance to Control the Structure of Chitosan Films and Their Protein Release Behavior. *AAPS PharmSciTech.* 2017, *18*, 1070–1083. DOI: [10.1208/s12249-016-0678-9](https://doi.org/10.1208/s12249-016-0678-9).
- [67] Ferrero, F.; Periolatto, M. Antimicrobial Finish of Textiles by Chitosan UV-Curing. *J. Nanosci. Nanotechnol.* 2012, *12*, 4803–4810. DOI: [10.1166/jnn.2012.4902](https://doi.org/10.1166/jnn.2012.4902).
- [68] Lazaridou, M.; Christodoulou, E.; Nerantzaki, M.; Kostoglou, M.; Lambropoulou, D. A.; Katsarou, A.; Pantopoulos, K.; Bikiaris, D. N. Formulation and in-Vitro Characterization of Chitosan-Nanoparticles Loaded with the Iron Chelator Deferoxamine Mesylate (DFO). *Pharmaceutics*. 2020, *12*, 238. DOI: [10.3390/pharmaceutics12030238](https://doi.org/10.3390/pharmaceutics12030238).
- [69] Bergonzi, C.; Di Natale, A.; Zimetti, F.; Marchi, C.; Bianchera, A.; Bernini, F.; Silvestri, M.; Bettini, R.; Elviri, L. Study of 3D-Printed Chitosan Scaffold Features after Different Post-Printing Gelation Processes. *Sci. Rep.* 2019, *9*, 362. DOI: [10.1038/s41598-018-36613-8](https://doi.org/10.1038/s41598-018-36613-8).
- [70] Abasalizadeh, F.; Moghaddam, S. V.; Alizadeh, E.; Akbari, E.; Kashani, E.; Fazljou, S. M. B.; Torbati, M.; Akbarzadeh, A. Alginate-Based Hydrogels as Drug Delivery Vehicles in Cancer Treatment and Their Applications in Wound Dressing and 3D Bioprinting (Journal of Biological Engineering (2020) 14: 8. *J. Biol. Eng.* 2020, *14*, 8. DOI: [10.1186/s13036-020-00239-0](https://doi.org/10.1186/s13036-020-00239-0).
- [71] Rokhathi, N.; Susanto, H.; Haryani, K.; Pramudono, B. Enhanced Enzymatic Hydrolysis of Chitosan by Surfactant Addition. *Period. Polytech. Chem. Eng.* 2017, *62*, 286–291. DOI: [10.3311/PPCh.11142](https://doi.org/10.3311/PPCh.11142).
- [72] Long, J.; Etxeberria, A. E.; Nand, A. V.; Bunt, C. R.; Ray, S.; Seyfoddin, A. A 3D Printed Chitosan-Pectin Hydrogel Wound Dressing for Lidocaine Hydrochloride Delivery. *Mater. Sci. Eng. C Mater. Biol. Appl.* 2019, *104*, 109873. DOI: [10.1016/j.msec.2019.109873](https://doi.org/10.1016/j.msec.2019.109873).
- [73] Varkey, M.; Visscher, D. O.; Van Zuijlen, P. P. M.; Atala, A.; Yoo, J. J. Skin Bioprinting: The Future of Burn Wound Reconstruction? *Burns Trauma*. 2019, *7*, 4. DOI: [10.1186/s41038-019-0142-7](https://doi.org/10.1186/s41038-019-0142-7).
- [74] Berger, J.; Reist, M.; Mayer, J. M.; Felt, O.; Peppas, N. A.; Gurny, R. Structure and Interactions in Covalently and Ionically Crosslinked Chitosan Hydrogels for Biomedical Applications. *Eur. J. Pharm. Biopharm.* 2004, *57*, 19–34. DOI: [10.1016/S0939-6411\(03\)00161-9](https://doi.org/10.1016/S0939-6411(03)00161-9).

- [75] Del Valle, E. M. M. Cyclodextrins and Their Uses: A Review. *Process Biochem.* 2004, 39, 1033–1046. DOI: [10.1016/S0032-9592\(03\)00258-9](https://doi.org/10.1016/S0032-9592(03)00258-9).
- [76] Sriamornsak, P.; Thirawong, N.; Weerapol, Y.; Nunthanid, J.; Sungthongjeen, S. Swelling and Erosion of Pectin Matrix Tablets and Their Impact on Drug Release Behavior. *Eur. J. Pharm. Biopharm.* 2007, 67, 211–219. DOI: [10.1016/j.ejpb.2006.12.014](https://doi.org/10.1016/j.ejpb.2006.12.014).
- [77] Yang, Y.; Zhao, W.; He, J.; Zhao, Y.; Ding, F.; Gu, X. Nerve Conduits Based on Immobilization of Nerve Growth Factor onto Modified Chitosan by Using Genipin as a Crosslinking Agent. *Eur. J. Pharm. Biopharm.* 2011, 79, 519–525. DOI: [10.1016/j.ejpb.2011.06.008](https://doi.org/10.1016/j.ejpb.2011.06.008).